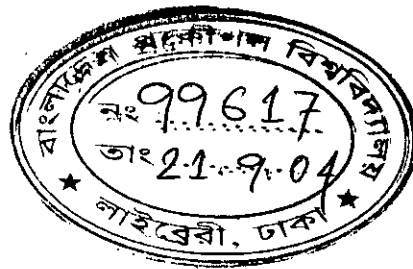


An Analytical Study of Critical Heat Flux
in
Natural Convective Boiling in a Vertical Tube

by

Hasan Mohammad Mostofa Afroz



MASTER OF SCIENCE IN MECHANICAL ENGINEERING

Department of Mechanical Engineering
Bangladesh University of Engineering & Technology
Dhaka-1000, Bangladesh

2004



#99617#

**An Analytical Study of Critical Heat Flux
in
Natural Convective Boiling in a Vertical Tube**

by

Hasan Mohammad Mostofa Afroz

A Thesis Submitted to the Department of Mechanical Engineering, Bangladesh University of Engineering & Technology, Dhaka in Partial Fulfillment of the Requirement for the Degree of Master of Science in Mechanical Engineering

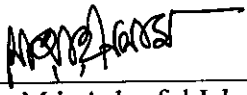
**Department of Mechanical Engineering
Bangladesh University of Engineering & Technology
Dhaka-1000, Bangladesh**


2004

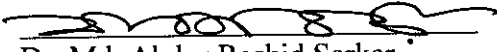
Certificate of Thesis Approval

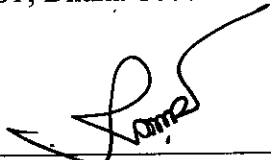
The thesis titled **An Analytical Study of Critical Heat Flux in Natural Convective Boiling in a Vertical Tube** submitted by **Hasan Mohammad Mostofa Afroz** Roll No: 100110017P Session: October 2001 has been accepted as satisfactory in partial fulfillment of the requirement for the degree of **Master of Science in Mechanical Engineering** on 31 August 2004.


BOARD OF EXAMINERS

1. 

Dr. Md. Ashraful Islam
Associate Professor
Department of Mechanical Engineering
BUET, Dhaka-1000. Chairman
(Supervisor)
2. 

Dr. Md. Quamrul Islam
Professor and Head
Department of Mechanical Engineering
BUET, Dhaka-1000. Member
(Ex-Officio)
3. 

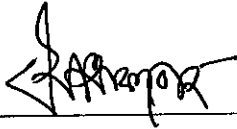
Dr. Md. Abdur Rashid Sarkar
Professor
Department of Mechanical Engineering
BUET, Dhaka-1000. Member
4. 

Dr. Chowdhury Md. Feroz
Professor
Department of Mechanical Engineering
BUET, Dhaka-1000. Member
5. 

Dr. Syeda Sultana Razia
Assistant Professor
Department of Chemical Engineering
BUET, Dhaka-1000. Member
(External)

DECLARATION

It is hereby declared that this thesis or any part of it has not been submitted elsewhere for the award of any degree or diploma.



Hasan Mohammad Mostofa Afroz

Student No. 100110017P

CONTENTS

	List of Figures and Tables	vii
	Nomenclature	ix
	Acknowledgements	xi
	Abstract	xii
CHAPTER	1 INTRODUCTION	1-4
	1.1 Motivation	1
	1.2 Objectives	4
CHAPTER	2 LITERATURE REVIEW	5-17
	2.1 General Concepts of CHF	5
	2.2 Experimental Studies on CHF	8
	2.3 Theoretical Studies on CHF	13
	2.4 Closure	17
CHAPTER	3 ANALYSIS METHODOLOGY	18-36
	3.1 Basic Model and Assumptions	18
	3.2 Governing Equations	19
	3.3 Solution Procedure	35
	3.4 Ranges of the Analysis	36
	3.5 Closure	36
CHAPTER	4 RESULTS AND DISCUSSIONS	37-51
	4.1 CHF Characteristics	37
	4.2 Effects of Pressure on CHF	40
	4.3 Effects of Tube Heating Length and Diameter Ratio	42
	4.4 Effects of Tube Heating Length on CHF	42
	4.5 Effects of Tube Diameter on CHF	44

	4.6	Effects of Liquid-Vapor Interface Profile Index	45
	4.7	Effects of Working Fluids on CHF	47
	4.8	Verification of the Present Model	48
	4.9	Closure	51
CHAPTER	5	CONCLUSIONS	52-53
	5.1	Conclusions	52
	5.2	Recommendations	53
		REFERENCES	54-60
		APPENDICES	61-76
APPENDIX	A	Thermo-Physical Properties of Working Fluids	62
APPENDIX	B	Flowchart and Program Code	63
APPENDIX	C	Experimental and Analytical Data Sample	70

LIST OF FIGURES AND TABLES

		Page No.
Fig. 2.1	Flow regimes and boiling mechanisms for upflow convective boiling in a vertical tube.	6
Fig. 2.2	Boiling regimes for a constant wall heat flux condition.	6
Fig. 2.3	Boiling regimes for an isothermal tube wall condition.	7
Fig. 2.4	Film dryout and the transition from annular to mist flow.	7
Fig. 2.5	Predicted CHF condition for water at 29.5 bar based on data by the USSR Academy of Sciences.	10
Fig. 2.6	Predicted CHF condition for water at 69 bar based on data by the USSR Academy of Sciences.	10
Fig. 2.7	Macrolayer dryout model schematic proposed by Haramura and Katto.	15
Fig. 3.1	Idealized flow model of the analysis of CHF	19
Fig. 3.2	Velocity profile of liquid at inlet	23
Fig. 3.3	Liquid-vapor interface profile length variation	25
Fig. 3.4	Liquid velocity variation for $L > L_{hc}$	25
Fig. 3.5	Liquid velocity variation for $L = L_{hc}$	26
Fig. 3.6	Liquid velocity variation for $L < L_{hc}$	27
Fig. 4.1	Characteristics of the CHF of natural convective boiling of saturated liquid in vertical tubes (analytical)	38
Fig. 4.2	Characteristics of the CHF of natural convective boiling of saturated liquid in vertical tubes (Experimental, [31])	38
Fig. 4.3	Effect of working pressure, P on CHF	40
Fig. 4.4	Effect of L_{hc}/D on CHF for R113	41
Fig. 4.5	Effect of L_{hc}/D on CHF for R12	41
Fig. 4.6	Effect of L_{hc}/D on CHF for Water	42

Fig. 4.7	Effect of tube heating length, L_{he} on CHF for R113	43
Fig. 4.8	Effect of tube heating length, L_{he} on CHF for R12	43
Fig. 4.9	Effect of tube diameter, D on CHF for R113	44
Fig. 4.10	Effect of tube diameter, D on CHF for R12	44
Fig. 4.11	Effects of profile index 'n' on the liquid-vapor interface shape	45
Fig. 4.12	Effect of profile index 'n' on CHF at different pressure	46
Fig. 4.13	Effect of profile index, n on CHF	46
Fig. 4.14	Effect of working fluid on CHF	47
Fig. 4.15	Comparison between analytical and experimental CHF for R113	48
Fig. 4.16	Comparison between analytical and experimental CHF for R12	49
Fig. 4.17	Comparison between analytical and experimental CHF for water	49
Fig. 4.18	Dependence of the present model on L_{he}/D	50
Fig. C.1	Contour plot of F1	75
Fig. C.2	Contour plot of F2	76
Table 3.1	Ranges of geometry and thermal-hydraulic conditions for the analysis	36
Table A.1	Thermo-physical properties of working fluids	62
Table C.1	Analytical and experimental CHF data for R113 at n=2	70
Table C.2	Analytical and experimental CHF data for R12 at n=2	70
Table C.3	Analytical and experimental CHF data for Water at n=2	71

NOMENCLATURE

A	Cross sectional area of the tube [m ²]
A _l	Cross sectional area of the liquid column [m ²]
A _v	Cross sectional area of the vapor column [m ²]
C _{fw}	Wall friction factor
D	Tube diameter [m]
D*	$= \frac{D}{\sqrt{\sigma/g(\rho_l - \rho_v)}}$
G	Mass flux [kg/m ² s]
G _{max}	Maximum mass flux at the CHF [kg/s.m ²]
g	Gravitational acceleration [m/s ²]
H _{lg}	Latent heat of evaporation [kJ/kg]
h _l	Heat transfer coefficient for the liquid phase
h _v	Heat transfer coefficient for the vapor phase
j _l	Superficial liquid velocity [m/s]
k _l	$= \frac{25\pi}{21}$, constant for calculating rate of change of momentum
Ku	Kutateladze number $\left[= \frac{q_{co} / \rho_v H_{lg}}{\sqrt[4]{\sigma g (\rho_l - \rho_v) / \rho_v^2}} \right]$
k _v	$= \frac{50\pi}{49}$, constant for calculating rate of change of momentum
L	Liquid-vapor interface profile length [m]
L _{he}	Tube heating length [m]
L ⁺	L _{he} /L
n	Liquid-vapor interface profile index
P	System pressure [MPa]

P_c	Critical pressure
P_r	Reduced pressure [= P/P_c]
P_l	Liquid pressure [MPa]
P_v	Vapor pressure [MPa]
q''	Heat flux [W/m^2]
q_{co}	CHF for saturated boiling [kW/m^2]
Re_l	Reynolds number for liquid
r	Radial coordinate of the tube
r_o	Radius of the tube [m]
u_l	Velocity of liquid [m/s]
u_v	Velocity of vapor [m/s]
x	Mass quality
x_{crit}	Dryout quality
z	Vertical coordinate along the tube
z^+	z/L

Greek Symbols

ρ_l	Density of liquid [kg/m^3]
ρ_v	Density of vapor [kg/m^3]
σ	Surface tension at vapor-liquid interface [N/m]
τ_i	Interfacial shear stress [N/m^2]
τ_w	Wall shear stress [N/m^2]
α	Void fraction [= A_v/A] or [= $(z/L)^{2/n}$]
μ_l	Viscosity of the liquid [Pa.s]

Subscripts

co	Critical condition in saturated boiling
fw	Wall friction
i	Liquid-vapor interface
l	Liquid
lg	Liquid-vapor phase change
v	Vapor
w	Wall

ACKNOWLEDGEMENTS

The author would like to express the heartiest gratitude and indebtedness to Dr. Ashraful Islam, Associate Professor, Department of Mechanical Engineering, Bangladesh University of Engineering and Technology, Dhaka for his guidance, supervision and moral supports throughout the entire period of this work. His patiently care and attention, valuable suggestions and encouragement are also gratefully acknowledged. Special thanks are due to Prof. Md. Quamrul Islam, Prof. Md. Abdur Rashid Sarkar, Prof. Chowdhury Md. Feroz and Dr. Syeda Sultana Razia for kindly examining the manuscript and offering valuable comments.

The author acknowledges his gratefulness to the Head, Department of Mechanical Engineering, BUET for providing required facilities. The author wishes to say “Thanks” to all staffs of Mechanical Department for their kind assistance.

The author wishes to express thanks and regards to the Vice-Chancellor and Head of the Department of Mechanical Engineering, DUET to give him permission to conduct research at M.Sc. level and for offering all sorts of assistance.

ABSTRACT

An analytical study has been made for the prediction of Critical Heat Flux (CHF) of natural convective boiling in a vertical uniformly heated tube, submerged in a saturated liquid bath by a flow model in which the CHF has treated to be occurred under annular co-current flow of liquid and vapor. Mass, momentum and energy balances for the two-phase (liquid-vapor) flow in a vertical tube are used to construct the flow model together with the criterion that the CHF is assumed to be taken place at the exit of the heated tube when void fraction is unity and mass flux is maximum. CHF data are calculated for saturated Water, R113 and R12 at different pressures of $P = 0.1$ to 3.0 MPa for the tube diameter of $D = 1.12$ to 18.4 mm, and the tube heating length of $L_{he} = 23$ to 960 mm. The effects of the pressure which corresponds to the density ratio ρ_v/ρ_l ranging from 0.622×10^{-4} to 0.2095 and of the ratio of $L_{he}/D = 5$ to 857 on the CHF, are mainly discussed. The characteristics of the CHF are satisfactorily explained against different parameters. About 300 predicted CHF data are compared with available experimental data to verify the basic performance of the model. The comparison shows that the predicted results by the present model agree with the experimental data within $\pm 50\%$ for the $L_{he}/D > 20$.



INTRODUCTION

1.1 MOTIVATION

Dissipation of large heat fluxes at relatively small temperature differences is possible in systems utilizing boiling phenomenon as long as the heated wall remains wetted with the liquid. With the wetted wall condition at the heated surface, heat is transferred by a combination of two mechanisms: (i) bubbles are formed at the active nucleation cavities on the heated surface, and heat is transferred by the nucleate boiling mechanism, and (ii) heat is transferred from the wall to the liquid film by convection and goes into the bulk liquid or causes evaporation at the liquid-vapor interface. But the removal or depletion of liquid from the heated wall leads to a sudden degradation in the heat transfer rate. The way in which the heated surface arrives at the liquid starved condition in a boiling system determines whether it is termed as Critical Heat Flux or Dryout condition. The evolution of the terminology itself is quite interesting. From a mechanistic viewpoint, the following definitions seem to be appropriate.

Critical Heat Flux (Departure from Nucleate Boiling) condition represents the upper limit of heat flux (in heat flux controlled systems) followed by a drastic rise in wall temperature, or considerable degradation in heat flux with an increase in wall temperature (in temperature controlled systems) in the nucleate boiling heat transfer. A vapor blanket covers the heated surface separating the surface from the liquid.

Dryout (Critical Heat Flux in Annular Flow Regime) condition represents the termination of continuous liquid contact with the wall. It follows the gradual depletion of liquid due to evaporation and entrainment of the liquid film. The vapor, from the continuous vapor phase in the bulk flow, covers the heated surface, and the discrete liquid droplets flowing in the vapor core may make occasional contact with the heated surface.

As early as 1888, Lang [1] recognized through his experiments with high pressure water that as the wall temperature increased beyond a certain point, it resulted in a reduction in heat flux. However, it was Nukiyama [2] who realized in 1934 that “the maximum heat transmission rate” might occur at relatively modest temperature differences. An excellent summary of the historical developments in this area was presented by Drew and Mueller [3] in 1937. Another aspect of historical significance is the evolution of the term Critical Heat Flux. Early investigators used various terminologies to describe this condition, e.g., maximum or peak heat flux, maximum boiling rate (Drew and Mueller [3]), and burnout heat flux. Nukiyama [2] described it as the critical point on the boiling curve. The earliest usage of the term Critical Heat Flux is seen in the work of Zuber [4] in 1959. Further investigation is needed to determine if publications in other languages (by investigators such as Kutateladze and Fritz) used this terminology. In the mid-1980s, the term Critical Heat Flux, and its acronym, CHF, became widely accepted.

The major impetus for the CHF studies in the recent past was the nuclear reactor core cooling. The catastrophic nature of the disaster associated with the CHF in a nuclear reactor, leading to core meltdown, put a high premium on the CHF studies. The urgency of the problem led to exhaustive experimentation in geometries similar to the reactor core. The safe operating limits were established through compilation of data from various experiments – developing the lookup tables. In his exhaustive literature survey report, Boyd [5-6] points out the severe inadequacies in the theoretical modeling of the CHF phenomena leading to empiricism.

Another major impetus for research in CHF was provided by the refrigeration and power industry in determining the dryout point in an evaporator and the safe operating limit in a boiler. The concerns in these cases were largely regarding safety and economic optimization of the systems. The focus for CHF and dryout studies as

we enter the new millennium has somewhat shifted. The issues related to the nuclear industries are still valid. However, the emphasis has now moved toward gaining the basic understanding of the mechanisms leading to the CHF condition. In the present days, enormous data and various empirical, semi-empirical correlations for CHF are available for each application. However, the applicable range of those correlations is geometrically and thermal-hydraulically confined to the experimental condition. The parametric trends are, however, identified from the data collected so far. A comprehensive theoretical model is yet to be developed.

In 1952, the most famous correlation of the CHF for ordinary pool boiling was developed by Kutateladze [7]. Compared with the pool boiling, both the theoretical and the experimental studies of the natural convective boiling in tubes and narrow channels are limited. Katto and Kurosaka [8] measured the CHF for three liquids (water, ethanol, and R113) in vertical annular channels. In 1993 Monde et al. [9] carried out an analytical study of the CHF of a two-phase thermosiphon, in which liquid and vapor form a counter current annular flow. Kodana and Kataoka [10] predicted forced convective CHF for DNB (Departure from Nucleate Boiling) type boiling transition that occurs inside of uniformly heated round tubes based on two-phase turbulence model. Their predicted CHF agreed well with experimental data, and the accuracy was within about 20%. Many more studies on CHF for various applications had been carried out in the past, from which the effect of various parameters on CHF can be understood. Some of them are described in the Literature Review (Chapter 2), which is devoted to the state-of-the art of CHF studies in general.

From the literature review it will be clear that very little analytical study on CHF of natural convective boiling have been carried out to obtain the fundamental design information necessary to apply the system as an efficient heat transfer device. Thus the present study is devoted to develop an analytical method to predict the CHF of natural convective boiling in vertical heated tubes, submerged in saturated liquid bath where liquid and vapor form a co-current flow and CHF is treated to be occurred at the exit of the heated tube with unit void fraction.

1.2 OBJECTIVES

The present work is of analytical type performed to understand the CHF mechanism in a vertical heated tube. Analysis is done for saturated water, R113 and R12 at various pressures to have ρ_v/ρ_l in the range of 0.622×10^{-4} to 0.2095 and by varying different geometrical parameters of the tube such as heating length of the tube, diameter of the tube, and also liquid–vapor interface profile index in order to fulfill the following objectives:

1. To obtain an analytical model for predicting CHF using mass, momentum and energy equations for the two phase (liquid–vapor) flow in the vertical tube together with the criterion that the CHF is assumed to be taken place at the exit of the heated tube when void fraction is unity.
2. To examine the effects of working fluid on the CHF
3. To examine the effects of tube diameter and heating length on the CHF
4. To examine the effects of working pressure on the CHF
5. To compare the analytical results with the experimental results, for similar geometry and thermal-hydraulic conditions.

LITERATURE REVIEW

2.1 GENERAL CONCEPT OF CHF

Saturated internal flow boiling is most often encountered in applications where complete or nearly complete vaporization of the coolant is desired. Perhaps the most frequently encountered example is the evaporator in a refrigeration or air conditioning system. Other examples include cryogenic processing applications, boilers in nuclear and conventional power plant systems, and chemical processing involving pure hydrocarbons. With the saturated film boiling regime the liquid film at the wall disappears due to evaporation and consequently the wall is exposed to vapor phase, which is termed as critical heat flux (dryout) in annular flow regime. In this case, heat transfer from the heating wall is suddenly deteriorated and wall temperature rapidly increases since the heated wall is almost covered by vapor phase.

Upward flow boiling in a vertical tube generally exhibits a sequence of vaporization mechanisms. As indicated schematically in Fig. 2.1, nucleate boiling is a major factor in the early stages of the vaporization process, where bubbly and slug flow occurs. Once churn or annular flow is attained, film evaporation usually becomes important. If the vaporization process continues, dryout of the liquid film will eventually occur, leaving vaporization of entrained droplets of liquid as the final stage of boiling process. The effect of varying heat flux or wall superheat on the flow and boiling mechanisms can be better understood by considering the boiling regime maps shown in Figs. 2.2 and 2.3 which are modified versions of a boiling regime map presented by Coiller [11]. As seen in Figs. 2.2 and 2.3, to avoid the high wall temperatures and/or the poor heat transfer associated with the saturated film-boiling

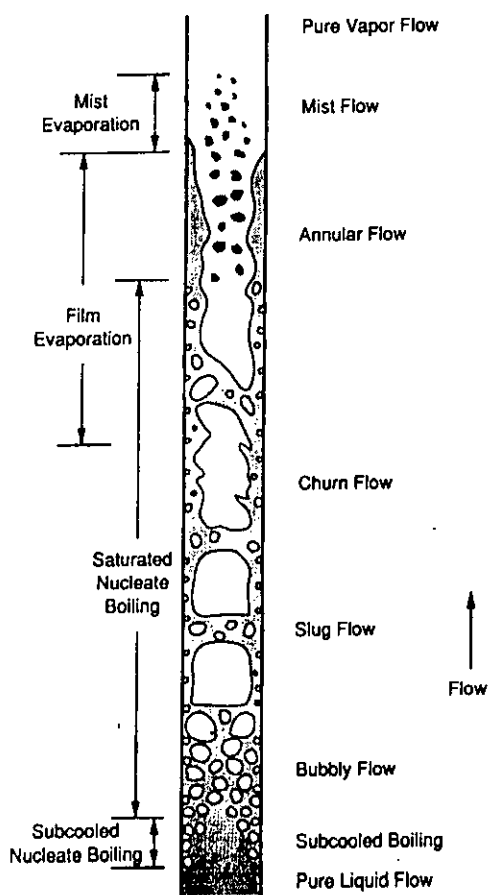


Fig. 2.1 Flow regimes and boiling mechanisms for upflow convective boiling in a vertical tube [12].

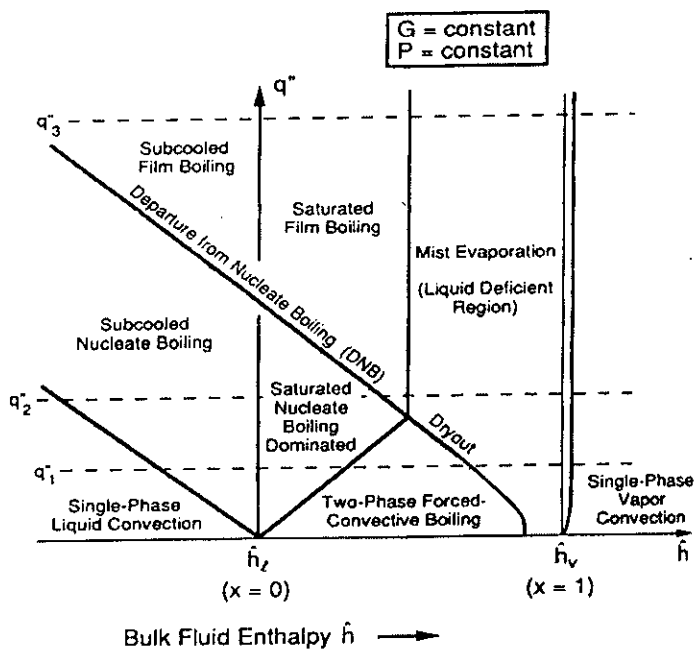


Fig. 2.2 Boiling regimes for a constant wall heat flux condition [12].

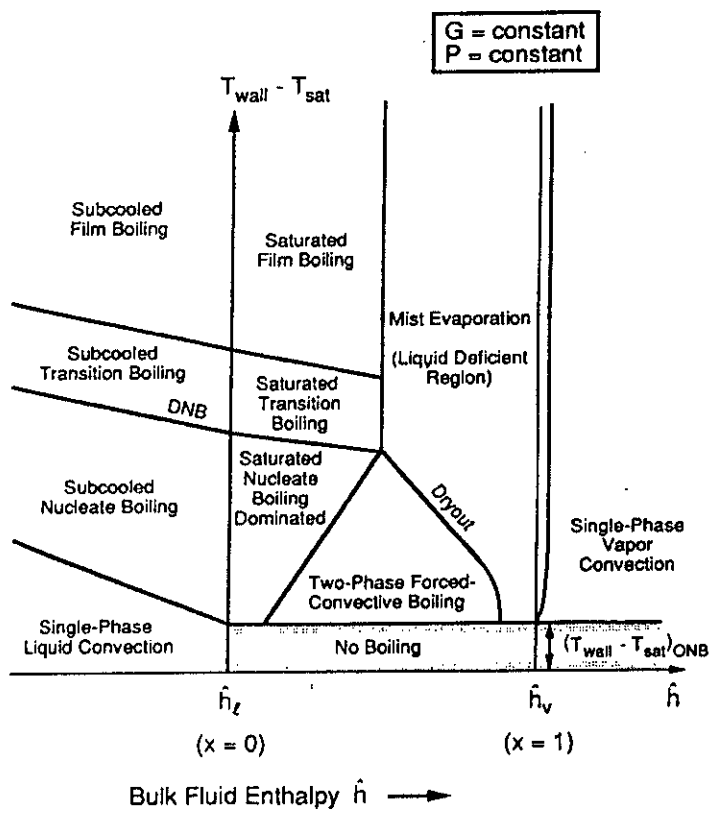


Fig. 2.3 Boiling regimes for an isothermal tube wall condition [12].

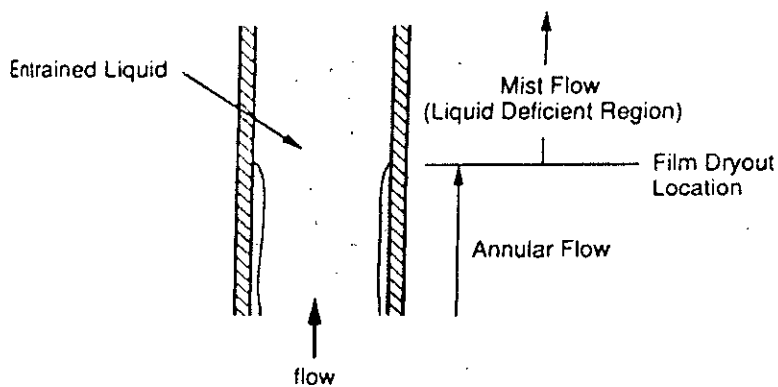


Fig. 2.4 Film dryout and the transition from annular to mist flow [12].

regime, the vaporization must be accomplished at low superheat or low heat flux levels. For this reason, evaporators and boilers are usually designed to avoid the high heat flux (CHF/Dryout) and high wall superheat levels of saturated flow boiling. Because most equipment operate in this range, so accurate prediction of critical heat flux due to the dryout of liquid film is particularly important from an engineering standpoint.

The critical heat flux condition is indicated schematically in Figs. 2.2 and 2.3 as diagonal lines. The nature of the transition indicated by these lines varies with the enthalpy of the flow. At subcooled (bulk flow) conditions and low qualities/low void fraction, this transition corresponds to a change in the boiling mechanism from nucleate to film boiling. For this reason, the critical heat flux condition for these circumstances is often referred to as the departure from nucleate boiling (DNB). In Soviet literature, this transition is referred to as burnout of the first kind.

At moderate to high qualities/void fraction, the flow is almost invariably in an annular configuration, and the transition corresponds to dryout of the liquid film on the tube wall (Fig.2.4). For this range of conditions, this transition is usually referred to simply as dryout. Most Soviet investigators have used the terminology burnout of the second kind for this transition. Once dryout occurs, the flow enters the so-called liquid-deficient region, in which the remaining liquid exists as entrained droplets.

2.2 EXPERIMENTAL STUDIES ON CHF

Although numerous investigations of critical heat flux conditions have been conducted, the mechanisms responsible for the critical heat flux transitions are not well understood yet. However, some light has been shed on the nature of these mechanisms. The complexity of these mechanisms has also made analytical modeling generally difficult. As a result, most proposed methods for predicting CHF conditions are some correlations based on experimental data.

Numerous CHF data were collected hitherto for different geometry. Bergles [13] has estimated that several hundred thousand CHF data points have been obtained so far, and that over 200 correlations have been developed in attempts to correlate the

data. Most of the available data have been obtained for upward flow boiling of water in a uniformly heated tube. The interested reader may wish to consult the summary of CHF data for water in vertical tubes compiled by Thompson and Macbeth [14] for further information.

With the large available database, evaluation of the data to eliminate questionable points is a formidable task. In the late 1960s, a group in the Soviet Union at the All-Union Heat Engineering Institute addressed this issue by reviewing available data. They subsequently tabulated recommended values of CHF conditions for upflow of water in a vertical tube with an inside diameter of 8 mm. These tabulated values were listed in a paper by Doroschuk and Lantsman [15]. This paper also described methods for extrapolating the CHF conditions to round tubes with different diameters. A more extensive tabulation, including DNB as well as dryout transitions, was published somewhat later by the heat and Mass Transfer section of the Scientific Council, USSR Academy of Sciences [16]. The tabulated CHF conditions were also for water in a vertical round tube with an inside diameter of 8mm, and the following method was recommended for predicting the CHF for other tube diameters:

$$q_{co} = (q_{co})_{8\text{mm}} \left(\frac{8}{D} \right)^{\frac{1}{2}} \quad (2.1)$$

Where D is the inside diameter in millimeters. These values of the CHF were plotted for two pressure levels in Figs.2.5 and 2.6. These figures clearly indicate the effects of varying system conditions on the CHF.

In general, for upward flow of water in a round tube, the parameters that may affect the critical heat flux include the mass flux G , the pressure P , the tube diameter D , the location z down stream of the tube inlet, and either the quality x or subcooling ($T_{\text{sat}} - T_{\text{bulk}}$). For sufficiently long tubes, the critical heat flux depends mainly on the four variables:

$$q_{co} = f(D, P, G, x_{\text{crit}}), \quad \text{for saturated flow} \quad (2.2)$$

$$q_{co} = f(D, P, G, T_{\text{sat}} - T_{\text{bulk}}), \quad \text{for subcooled flow} \quad (2.3)$$

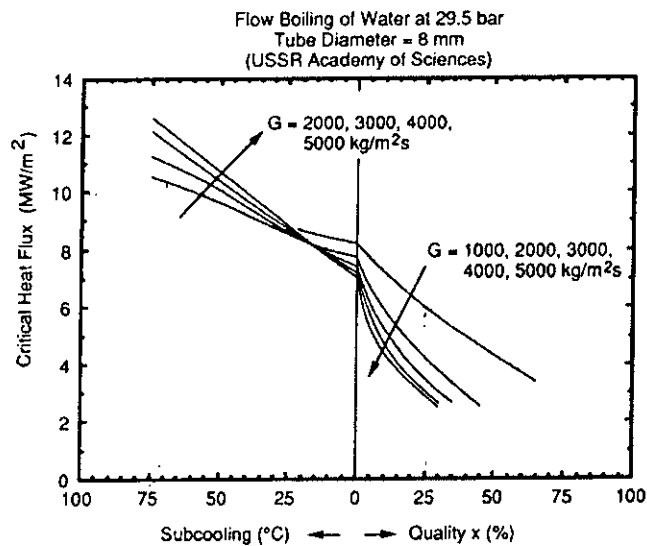


Fig. 2.5 Predicted CHF condition for water at 29.5 bar based on data by the USSR Academy of Sciences [12].

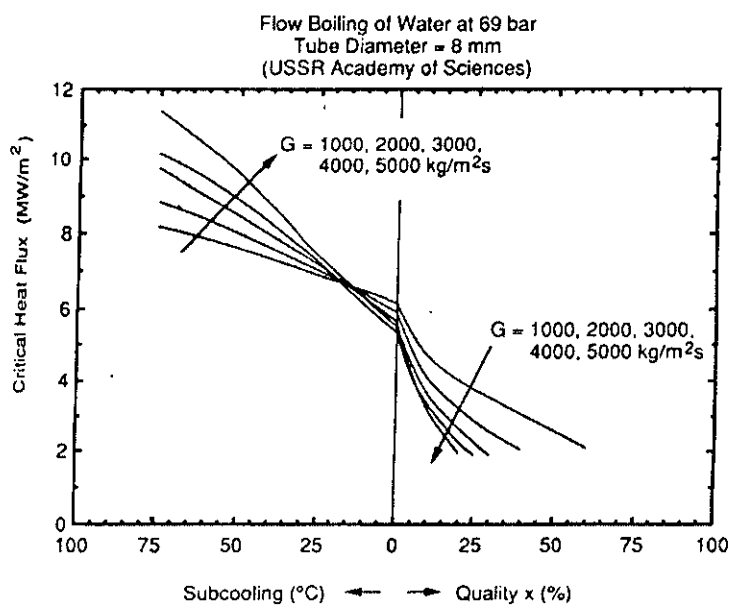


Fig. 2.6 Predicted CHF condition for water at 69 bar based on data by the USSR Academy of Sciences [12].

A relatively recent paper by Groeneveld et al. [17] presents the summary of the latest 1995 look-up table developed jointly by AECL Research (Canada) and IPEE (Obninsk, Russia). It is based on an extensive database of CHF values in tubes with vertical upflow of steam-water mixtures. The table is designed to provide CHF values for 8 mm diameter tubes at discrete values of pressure, mass flux, and dryout qualities. Linear interpolation is provided for intermediate values, with an empirical correction factor for diameters different from 8 mm. The look-up table provides a tool capable of predicting data with an rms error of 7.82 percent for the 22,946 data points.

A comprehensive paper by Nariai and Inasaka [18] presents a summary of their own experimental work and presents useful parametric relationships between CHF and important system variables. A comparison with the available correlations is also presented. A recent review of CHF fundamentals, models and correlation schemes is presented by Celata and Mariani [19]. They present a comprehensive summary of investigations of the CHF condition and reflect our current understanding of this phenomenon. Earlier review articles by Celata [20-21] provide a good overview of the models describing the CHF mechanism. Tong and Tang [22] present a very comprehensive summary of the available literature on various aspects of flow boiling crisis.

Building on earlier investigations by Thompson and Macbeth [14], Bowring [23] proposed an empirical correlation for the prediction of CHF in tubes with vertical up flow of steam-water mixtures. Collier reports that the root-mean square error for this correlation is 7%.

Biasi et al. [24] proposed the following CHF correlation scheme for vertical upflow boiling of water in uniformly heated tubes:

$$q''_{\text{crit}} = \frac{1883}{D^m G^{1/6}} \left[\frac{F_{\text{Bi}}(p)}{G^{1/6}} - x \right], \quad \text{For low qualities subcooled flow} \quad (2.4)$$

$$q''_{\text{crit}} = \frac{3780 H_{\text{Bi}}(p)}{D^m G^{0.6}} [1 - x], \quad \text{For high qualities saturated flow} \quad (2.5)$$

Where, $m = 0.4$ for $D \geq 1$ cm
 $m = 0.6$ for $D \leq 1$ cm

$$F_{Bi}(P) = 0.7249 + 0.099P \exp(-0.032P)$$

$$H_{Bi}(P) = -1.159 + 0.149P \exp(-0.019P) + 8.99P/(10 + P^2)$$

In these dimensional relations, D is in cm, P is in bar, G is in $\text{gm}/\text{cm}^2\text{s}$. The correlation is reported to be valid over ranges $10 < G < 600 \text{ gm}/\text{cm}^2\text{s}$, $2.7 < P < 140 \text{ bar}$, $0.3 < D < 3.75$, $20 < Z < 600 \text{ cm}$, $\rho_v/(\rho_l \rho_v) < x < 1$. The RMS error of this correlation against a database of over 4500 points was reported to be 7.3%.

The correlations discussed above are all for boiling of water. There is a need, however, for CHF prediction methods for other fluids as well. The best generalized correlation of CHF conditions in vertical, uniformly heated tubes is that recently proposed by Katto and Ohno [25] which is an updated version of the correlation proposed by Katto [26-27]. It attempts to correct some inconsistencies and improves the accuracy of the earlier version. It has been found to agree reasonably well with available data for boiling of water, R-12, R-22, and liquid helium for tube diameters near 10mm, and heated lengths near 1000mm.

Additional CHF prediction methods have also been proposed by Shah [28], Levy et al. [29], and Groeneveld et al. [30]. The correlation [30] is a simple tabulated correlation which provides a reasonably good fit to CHF data for water, R-11, R-12, R-21, R-113, R-114, CO_2 and N_2 .

Monde et al. [31] carried out an experimental study of CHF for natural convective boiling of saturated liquid in a vertical uniformly heated tube. The experiment was performed at a pressure of $P = 0.1$ to 3.1 MPa for the tube diameter of $D = 1.12$ to 18.4 mm , the tube length of $L_{he} = 23$ to 960 mm and three kinds of liquids (water, R-113, and R-12). The effects of the pressure which corresponds to the density ratio ρ_v/ρ_l ranging from 6.24×10^{-4} to 0.236 and of the ratio of $L_{he}/D = 5$ to 857 on the CHF were mainly examined. The experiment shows that the characteristics of the CHF can be divided into two regimes at a point that a nondimensional parameter of D^* is equal to about 13. The CHF data for $D^* < 13$ and $L_{he}/D < 240$ are predicted within an accuracy of $\pm 20\%$ by the following correlation:

$$\frac{q_{co} / \rho_v H_{lg}}{\sqrt[4]{\sigma g (\rho_l - \rho_v) / \rho_v^2}} = \frac{0.16}{1 + 0.025 \left(\frac{L_{he}}{D} \right)} \quad (2.6)$$

While for $D^* > 13$, the CHF data are predicted by the correlation:

$$\frac{q_{co} / \rho_v H_{lg}}{\sqrt[4]{\sigma g (\rho_l - \rho_v) / \rho_v^2}} = \frac{0.16}{1 + 0.003 \left(L_{he} / \sqrt{\sigma / g (\rho_l - \rho_v)} \right)} \quad (2.7)$$

The CHF for $D^* > 13$ is dependent on the tube length only in place of L_{he}/D .

2.3 THEORETICAL STUDIES ON CHF

Celata [19] summarizes the previous models for predicting CHF in the following five categories.

1. Boundary Layer Ejection Model
2. Critical Enthalpy in the Bubble Layer Model
3. Liquid Flow Blockage Model
4. Vapor Removal Limit and Near-wall Bubble Crowding Model, and
5. Liquid Sublayer Dryout Model

Boundary Layer Ejection Model. This model was originally proposed by Kutatleadze and Leont'ev [32]. The boiling mechanism is compared with the injection of a gas stream into liquid flow through a permeable plate. The ejection of bubbles into the mainstream is postulated to be the cause of the boundary layer separation at the heater surface. However, the photographic study conducted by Mattson et al. [33] does not show any abrupt changes in the macroscopic structure of the flow near the CHF location. The high velocity vapor ejection from the heater surface into the flow was also not observed.

Critical Enthalpy in the Bubble Layer Model. This model was proposed by Tong et al. [34]. They assume that a layer of small bubbles flowing adjacent to the heater surface traps the liquid between the bubble layer and the heated surface. This bubble layer separates the trapped superheated liquid layer from the mainstream. They

postulated that the CHF condition is reached when this superheated liquid layer attains a certain limiting enthalpy. This model does not provide a clear explanation of the CHF phenomenon other than stating the existence of a critical liquid enthalpy in the superheated liquid layer. Fiori and Bergles [35] suggest that, based on their observations, the CHF condition results from a periodic wall temperature rise followed by a disruption of the liquid film caused by nucleate boiling. Kirby et al. [36] observed such wall temperature behavior near the CHF location; however, the actual CHF mechanism is not clearly described by this model.

Liquid Flow Blockage Model. Bergel'son [37] proposed this model based on the assumption that the flow of the liquid toward the heated surface is blocked by the outflow of vapor from the heater surface. This behavior may be feasible under very low mass flux conditions where the liquid and vapor flow structure is similar to that in the case of pool boiling. However, the vapor flow away from the wall is not seen to be a limiting factor in subcooled flow boiling. Due to the inadequate evidence supporting this mechanism, this model is not being pursued by other researchers.

Vapor Removal Limit and Near-Wall Bubble Crowding Model. This model is based on the limit of the turbulent interchange between the bubbly layer and the bulk of the liquid, and the crowding of the bubbles preventing the liquid access to the heated wall [38]. Weisman and Pei [39] consider the existence of a bubbly layer adjacent to the wall at subcooled or low quality conditions. Although their model assumes the existence of a bubbly layer, the enthalpy transport from this bubbly layer to the bulk flow is considered as the limiting factor leading to the CHF condition. They consider the CHF to be a local phenomenon. The liquid region in the immediate vicinity of the heater fills with bubbles building a bubbly layer. In this region, the turbulent eddy size is insufficient to transport the bubbles away from the heater surface. At the CHF location, this layer is assumed to be at its maximum thickness. It is postulated that the CHF condition occurs when the volume fraction of vapor in the bubbly layer just exceeds the critical volume fraction at which an array of ellipsoidal bubbles can be maintained without significant contact between the bubbles. Weisman and Pei used the homogeneous flow model in the bubbly layer. The resulting model has three adjustable empirical constants that are evaluated from the experimental data.

This model includes the two-phase considerations that are readily extendable to the saturated flow conditions as well.

Liquid Sublayer Dryout Model. Katto and Yokoya [40] proposed a preliminary model describing the macrolayer dryout as the mechanism leading to CHF in pool boiling. Later, Haramura and Katto [41] completed the model development by introducing the mechanism for macrolayer formation in both pool and flow boiling. Further description of the pool boiling CHF model is given by Haramura [42]. Figure 2.7 shows a schematic of the macrolayer model. According to this model, as a result of the Helmholtz instability, the columnar structure of vapor stems collapses with a vapor film blanketing a thin liquid film on the heater surface. Numerous vapor stems emerge on the heater surface through this liquid film. Under flow conditions, both the liquid sublayer and the vapor film move in the flow direction. Entrainment and deposition phenomena are ignored because they are presumed to be scarce. Under these conditions, liquid is fed into the film from the upstream end, while it depletes along the flow direction due to evaporation. The CHF condition is reached when the heat supplied by the heater surface provides the necessary latent heat required to completely evaporate the liquid entering the film. Katto [43-44] provided a detailed description of the model based on the macrolayer evaporation. Their model uses several empirical constants in determining the liquid film thickness, the liquid film flow rate, and temperature of the liquid entering into the sublayer. Lee and Mudawar [45] considered the effect of velocity in the subcooled flow in terms of stretching the large bubble in the Haramura and Katto model to a vapor blanket of length equal to the critical Helmholtz wavelength. The vapor blanket separates the bulk flow from a thin sublayer trapped between the vapor blanket and the heated surface.

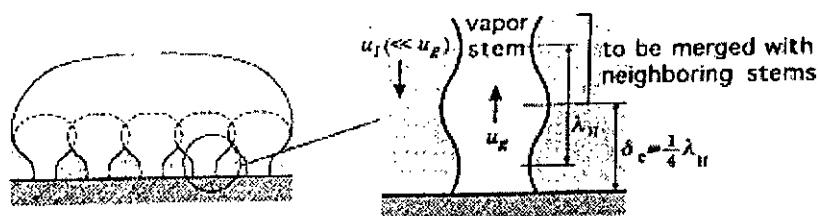


Fig. 2.7 Macrolayer dryout model schematic proposed by Haramura and Katto

The bubble moves at a velocity u_b while the sublayer moves at a velocity of u_m . The sublayer is depleted if the rate of evaporation from the sublayer exceeds the rate at which the sublayer is replenished due to the difference in velocities of the sublayer and the vapor blanket. The sublayer mass velocity, its thickness, and the vapor blanket length were calculated by considering the buoyancy and drag forces acting on the vapor blanket. Their modeling resulted in a correlation scheme with three empirical constants, which were determined from a large set of experimental data. Celata et al. [46] eliminated the empirical constants in the Katto, and Lee and Mudawar models by using the homogeneous flow model and by introducing appropriate correlations from available literature to calculate the sublayer thickness, flow rate, enthalpies, and vapor blanket length. However, the basic features of the model are similar to those proposed by Lee and Mudawar [45].

As mentioned earlier, for saturated conditions at moderate to high qualities, the critical heat flux condition most often corresponds to dryout of the liquid film on the tube wall. To predict the conditions at which dryout occurs, one approach would be to model the annular film flow evaporation process which would require analysis of the mass and momentum transport in the core flow and the liquid film on the tube wall and transport of heat across the liquid film and computationally predict the conditions at which the film thickness or the film flow rate goes to zero.

The condition at which the film dries out is largely dictated by the transport in the core and the film regions and the interaction of the mechanisms of deposition, entrainment, and vaporization. This approach for predicting the dryout condition is plausible because, at low to moderate heat flux levels, the entrainment and deposition mechanisms apparently are largely unaffected by the presence of the applied heat flux. This makes it possible to apply the entrainment/deposition models developed for adiabatic equilibrium annular flow with evaporation of the liquid film. An analysis of this type proceeds by integrating the transport equations in the core flow and in the film along the channel from known or assumed boundary conditions at the starting point to the point where the film thickness goes to zero. Dryout is thus determined as the point where the processes of evaporation, deposition, and entrainment lead to a condition in which the film flow rate becomes zero. Analytical treatments of this type have been explored in depth by Whalley, Hewitt, and co-workers [47-50]. The results

of these investigations indicate that this type of method can be used successfully to predict dryout conditions for forced-convective boiling in tubes, annuli, and rod bundles. For a further discussion of this method of predicting dryout conditions, the interested reader may wish to consult references [51-53].

Okawa [54] predicted CHF in annular flow using a film flow model. His predicted results agree with the experimental data fairly well when the flow of pattern at the onset of critical heat flux condition is considered annular flow. The predictive capability was not deteriorated even in the cases of small diameter tube, short length tube as well as low vapor quality. Good agreements were also achieved in the preliminary tests against the critical heat flux data for Freon12 and Freon21.

In the present analysis, the model considers mass, momentum, and energy balances for the two-phase co-current flow where the vapor forms a paraboloid and the CHF is assumed to be taken place at the exit of the heated tube where the mass flux is maximum. From the above literature review it is clear that the approach of the present analysis is not used so far by other existing analytical models.

2.4 CLOSURE

In this chapter, some fundamental principles of CHF have been presented surveying the literature available upto now. In addition, special attention has been given to the CHF mechanism in the vertical tube and all the available empirical correlations and theoretical models for predicting CHF are reviewed. In the following chapter, the analytical methodology for predicting the CHF during natural convective boiling in vertical tubes submerged in saturated liquids is described.

ANALYSIS METHODOLOGY

Flow model, assumptions, and necessary equations for predicting the CHF of natural convective boiling in a vertical tube are described in this chapter. The analysis ranges and the solution procedure are also mentioned in detail.

3.1 BASIC MODEL AND ASSUMPTIONS

An analytical study has been made for the prediction of CHF of natural convective boiling in a vertical uniformly heated tube, submerged in a saturated liquid bath. This analysis has been carried out by a flow model in which the CHF has treated to be occurred under annular co-current flow of liquid and vapor. The proposed model assumes the flow situation of liquid and vapor just before the CHF point as shown in the Fig. 3.1. The interface of the annular flow is a paraboloid formed by Eq. (3.1) where the exponent 'n' gives the shape of the interface.

$$\frac{z}{L} = \left(\frac{r}{r_o} \right)^n, \text{ for } n \geq 2 \quad (3.1)$$

The profile length, L may vary in such a way that it may be greater than, less than or equal to the tube heating length, L_{hc} as shown in the Fig. 3.3.

From Eq. (3.1) the void fraction, α , at any location can easily be obtained by:

$$\alpha = \left(\frac{r}{r_o} \right)^2 = \left(\frac{z}{L} \right)^{\frac{2}{n}} \quad (3.2)$$

The CHF is assumed to be taken place at the exit of the heated tube when the void fraction is unity. In addition to this assumption, both entrainment and deposition of liquid are ignored and the two phases are considered in local thermodynamic equilibrium and the flow is considered steady.

3.2 GOVERNING EQUATIONS

For deriving the necessary equations for this model, a control volume, abcd, is chosen as shown in the Fig. 3.1 bounded by dotted line.

In Fig. 3.1,

I \Rightarrow Control volume containing vapor

II \Rightarrow Control volume containing liquid

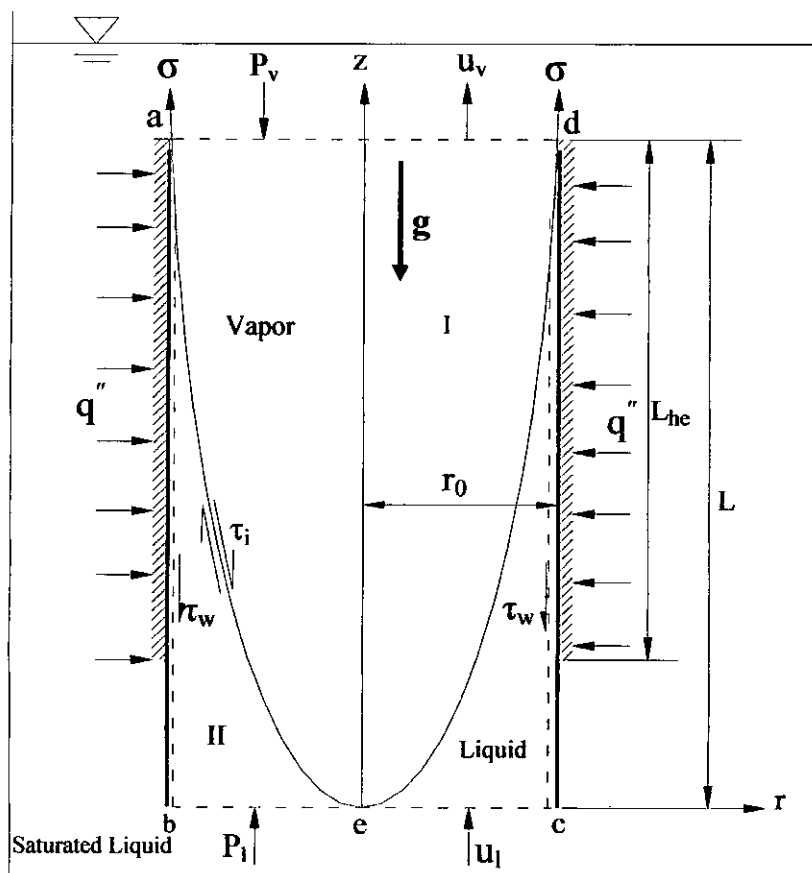


Fig. 3.1 Idealized flow model of the analysis of CHF

From the mass conservation equation, we get

$$\int_{\text{CSI}} \rho \bar{u} d\bar{A} = \int_{\text{CSII}} \rho \bar{u} d\bar{A} = 0 \quad (3.3)$$

The force-momentum balance of the control volume (I) in the z- direction can be expressed as-

$$-\int_{\text{CVI}} \rho_v g dV + \int_{\text{CSI}} P dA - 2\pi \int_0^L r(\tau_i)_I dz = \int_{\text{CSI}} (Gu)_{\text{out}} dA - \int_{\text{CSI}} (Gu)_{\text{in}} dA \quad (3.4)$$

And the force-momentum balance of the control volume (II) in the z- direction is –

$$-\int_{\text{CVII}} \rho_l g dV + \int_{\text{CSII}} P dA + 2\pi \int_0^L r(\tau_i)_{II} dz - \int_0^L 2\pi r_o \tau_w dz = \int_{\text{CSII}} (Gu)_{\text{out}} dA - \int_{\text{CSII}} (Gu)_{\text{in}} dA \quad (3.5)$$

For steady flow, the interfacial shear forces must be balanced. Adding Eq. (3.4) and Eq. (3.5) the following relation for the overall momentum balance of the control volume ‘abcd’ is obtained:

$$\left[\int_{\text{CSI}} P dA + \int_{\text{CSII}} P dA \right] - g \left[\int_{\text{CVI}} \rho_v dV + \int_{\text{CVII}} \rho_l dV \right] - \int_0^L 2\pi r_o \tau_w dz \quad (3.6)$$

$$= \int_{\text{CSI}} (Gu)_{\text{out}} dA - \int_{\text{CSII}} (Gu)_{\text{in}} dA$$

$$F_P - F_G - F_w - F_M = 0 \quad (3.7)$$

Where,

$$F_P = \left[\int_{\text{CSI}} P dA + \int_{\text{CSII}} P dA \right] \quad = \text{Pressure Force}$$

$$F_G = g \left[\int_{\text{CVI}} \rho_v dV + \int_{\text{CVII}} \rho_l dV \right] \quad = \text{Gravity Force}$$

$$F_w = \int_0^L 2\pi r_o \tau_w dz \quad = \text{Wall Friction Force}$$

$$F_M = \int_{\text{CSI}} (Gu)_{\text{out}} dA - \int_{\text{CSII}} (Gu)_{\text{in}} dA \quad = \text{Rate of Change of Momentum}$$

Now F_P , F_G , F_w , & F_M can be simplified as follows:

EVALUATION OF F_P

$$\begin{aligned}
 F_P &= \left[\int_{CS I} P dA + \int_{CS II} P dA \right] \\
 &= \int_{acd} P_1 dA - \int_{ad} P_v dA - \int_{acd} P_v dA + \int_{bc} P_1 dA \\
 &= \underbrace{\left[\int_{acd} P_1 dA - \int_{acd} P_v dA \right]}_{\text{Surface tension force}} + \underbrace{\left[\int_{bc} P_1 dA - \int_{ad} P_v dA \right]}_{\text{Buoyancy force}}
 \end{aligned}$$

$$\therefore F_P = 2\pi r_0 \sigma + \rho_l g \pi r_0^2 L$$

EVALUATION OF F_G

$$\begin{aligned}
 F_G &= g \left[\int_{CV I} \rho_v dV + \int_{CV II} \rho_l dV \right] \\
 &= g \left[\int_0^L \rho_v A_v dz + \int_0^L \rho_l A_l dz \right] \\
 &= Ag \left[\int_0^L \rho_v \frac{A_v}{A} dz + \int_0^L \rho_l \frac{A_l}{A} dz \right] \\
 &= \pi r_0^2 g \left[\int_0^L \rho_v \alpha dz + \int_0^L \rho_l (1 - \alpha) dz \right] \\
 &= \pi r_0^2 g \left[(\rho_v - \rho_l) \int_0^L \alpha dz + \rho_l \int_0^L dz \right] \\
 &= \pi r_0^2 g \left[(\rho_v - \rho_l) \int_0^L \left(\frac{z}{L} \right)^n dz + \rho_l \int_0^L dz \right]
 \end{aligned}$$

$$\therefore F_G = \pi r_0^2 g L \left[(\rho_v - \rho_l) \frac{n}{n+2} + \rho_l \right]$$

EVALUATION OF F_M

$$F_M = \int_{\text{CSI}} (G.u)_{\text{out}} dA - \int_{\text{CSII}} (G.u)_{\text{in}} dA$$

Here,

$$\int_{\text{CSI}} (G.u)_{\text{out}} dA = \int_0^{r_0} \rho_v u_v^2 2\pi r dr,$$

$$= \int_0^{r_0} 2\pi r \rho_v u_{\text{max}}^2 \left(1 - \frac{r}{r_0}\right)^{\frac{2}{7}} dr, \quad \left[\text{as } u_v(r) = u_{\text{max}} \left(1 - \frac{r}{r_0}\right)^{\frac{1}{7}} \right]$$

$$\therefore \int_{\text{CSI}} (G.u)_{\text{out}} dA = 2\pi \rho_v u_{\text{max}}^2 I_1, \quad \text{Let, } I_1 = \int_0^{r_0} r \left(1 - \frac{r}{r_0}\right)^{\frac{2}{7}} dr$$

Substituting $1 - \frac{r}{r_0} = z$, we get

$$I_1 = \frac{49}{144} r_0^2$$

$$u_{\text{mean}} = \frac{\text{Total volume per unit time passing through the section}}{\text{Total area of cross section}}$$

$$\begin{aligned} u_{\text{mean}} &= \frac{1}{\pi r_0^2} \int_0^{r_0} u_v dA_v \\ &= \frac{1}{\pi r_0^2} \int_0^{r_0} u_{\text{max}} 2\pi r \left(1 - \frac{r}{r_0}\right)^{\frac{1}{7}} dr \end{aligned}$$

Considering $1 - \frac{r}{r_0} = z$, we get

$$\therefore u_{\text{mean}} = 2u_{\text{max}} \int_0^1 (1-z) z^{\frac{1}{7}} dz$$

$$\therefore u_{\text{max}}^2 = \frac{60^2}{49^2} u_{\text{mean}}^2$$

$$u_{\text{max}}^2 = \frac{60^2}{49^2} \frac{G^2}{\rho_v^2},$$

$$\text{as } [G = \rho_v u_{\text{mean}}]$$

Using the value of I_1 and u_{max} we get,

$$\int_{\text{CSI}} (G.u)_{\text{out}} dA = \frac{50}{49} \pi r_0^2 \frac{G^2}{\rho_v}$$

$$\Rightarrow \int_{\text{CSI}} (G.u)_{\text{out}} dA = k_v r_0^2 \frac{G^2}{\rho_v}, \quad \text{Where, } k_v = \frac{50}{49} \cdot \pi$$

Again, $\int_{\text{CSII}} (G.u)_{\text{in}} dA$ can be analyzed by the following way,

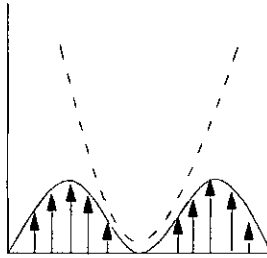


Fig. 3.2 Velocity profile of liquid at inlet

Let the inlet velocity profile for liquid is

$$u_1(r) = A + Br + Cr^2 + Dr^3 \quad (3.8)$$

With boundary conditions,

$$(i) r = 0, \quad u = 0$$

$$(ii) r = 0, \quad \frac{\partial u}{\partial r} = 0$$

$$(iii) r = r_0, \quad u = 0$$

Applying boundary conditions in (3.8), we get,

$$u_1(r) = -Dr_0 r^2 + Dr^3$$

Again if \bar{U} be the mean velocity at the inlet, then,

$$\begin{aligned} \pi r_0^2 \bar{U} &= \int_0^{r_0} 2\pi r \cdot u(r) \cdot dr \\ &= 2\pi D \int_0^{r_0} (r^4 - r_0 r^3) dr \end{aligned}$$

$$\therefore D = \frac{-10\bar{U}}{r_0^3}$$

$$\therefore u_1(r) = 10\bar{U} \cdot \left(\frac{r}{r_0}\right)^2 \cdot \left(1 - \frac{r}{r_0}\right)$$

$$\therefore \int_{CSII} (Gu)_{in} dA = \int_0^{r_0} 2\pi \rho_l u_l^2 r dr \quad \text{as } G_l = \rho_l u_l$$

$$= 2\pi \rho_l \int_0^{r_0} \left[10\bar{U} \left(\frac{r}{r_0} \right)^2 \left(1 - \frac{r}{r_0} \right) \right]^2 r dr \quad \text{as } \bar{U} = \frac{G}{\rho_l}$$

$$= \frac{25}{21} \left(\pi r_0^2 \right) \cdot \frac{G^2}{\rho_l}$$

$$\int_{CSII} (G.u)_{in} dA = k_l \frac{r^2 G^2}{\rho_l}, \quad \text{Here, } k_l = \frac{25}{21} \cdot \pi$$

$$\therefore F_M = \left(\frac{k_v}{\rho_v} - \frac{k_l}{\rho_l} \right) r_0^2 \cdot G^2$$

EVALUATION OF F_w

$$F_w = \int_0^L 2\pi r_0 \tau_w dz$$

$$\tau_w = \frac{1}{2} C_{fw} \rho_l u_l^2 = \frac{1}{2} C_{fw} \rho_l \frac{j_l^2}{(1-\alpha)^2}, \quad \text{as } j_l = (1-\alpha)u_l$$

$$\therefore F_w = \pi r_0 \rho_l \int_0^L C_{fw} \frac{j_l^2}{(1-\alpha)^2} dz \quad (3.9)$$

C_{fw} , the wall friction factor, can be obtained from the equations provided by Wallis [58] in the laminar and turbulent flow regions and by Monde [57] in the transition regions as follows-

$$C_{fw} = \frac{16}{Re_l}, \quad \text{When, } Re_l \leq 160 \quad (3.10a)$$

$$C_{fw} = \text{Exp} \left[5.48616 - 2.10284 \log_c (Re_l) + 0.11855 (\log_c Re_l)^2 - 1.30035 \times 10^{-3} (\log_c Re_l)^3 \right], \quad \text{when, } 160 \leq Re_l \leq 10^4 \quad (3.10b)$$

$$C_{fw} = 0.079 / Re_l^{-0.25}, \quad \text{When, } Re_l \geq 10^4 \quad (3.10c)$$

The value of C_{fw} depends on Reynolds number, which again depends on the liquid property and velocity. The variation of the superficial liquid velocity, j_l along the

length of the tube can be analyzed as follows-

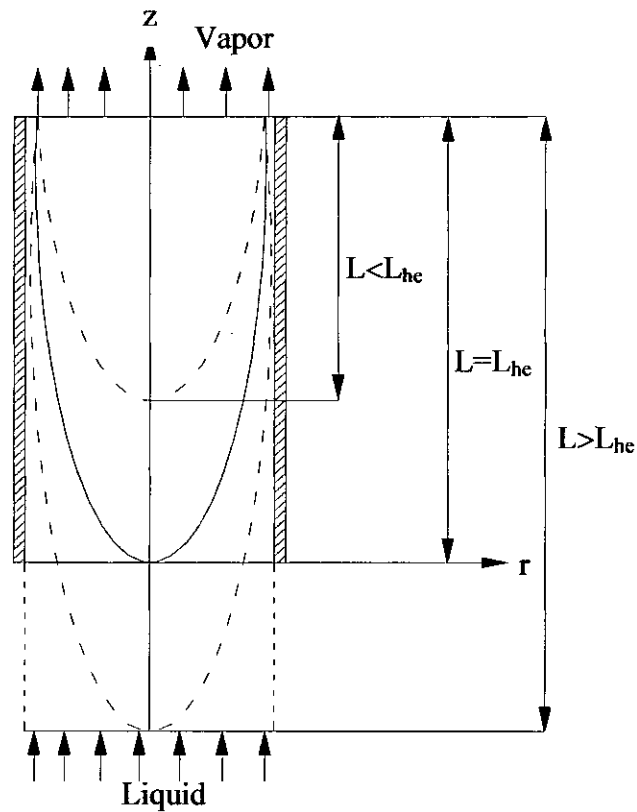


Fig. 3.3 Liquid-vapor interface profile length variation

For $L > L_{he}$ or $\left[L^+ = \frac{L_{he}}{L} < 1 \right]$

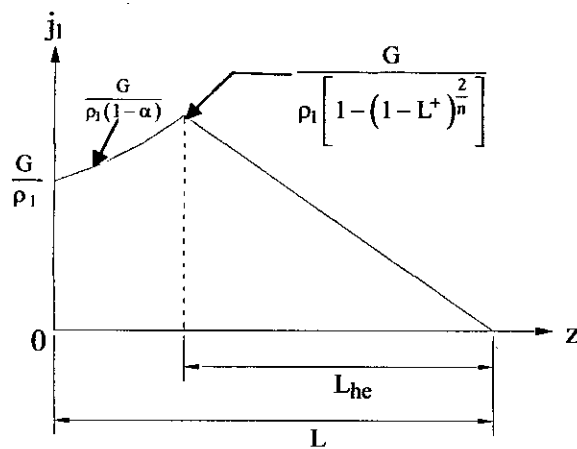


Fig. 3.4 Liquid velocity variation for $L > L_{he}$

For $z=0$ to $(L-L_{hc})$ liquid enters into the main flow from the side because tube wall is not exist there, so that increasing j_l is seen in this region as $j_l = \frac{G}{\rho_l(1-\alpha)}$.

$$\therefore j_l = \frac{G}{\rho_l \left(1 - z^{+\frac{2}{n}}\right)}, \quad 0 \leq z^+ \leq 1 - L^+ \quad (3.11)$$

And,

$$j_l = \frac{G(1-z^+)}{\rho_l \left[1 - (1-L^+)^{\frac{2}{n}}\right] L^+}, \quad 1 - L^+ \leq z^+ \leq 1 \quad (3.12)$$

$$\therefore Re_f = \frac{\rho_l \cdot j_l \cdot D}{\mu_l} = \frac{G \cdot D}{\mu_l \left[1 - z^{+\frac{2}{n}}\right]}, \quad 0 \leq z^+ \leq 1 - L^+ \quad (3.13)$$

And

$$Re_f = \frac{G \cdot D \cdot (1-z^+)}{\mu_l \left[1 - (1-L^+)^{\frac{2}{n}}\right] L^+}, \quad 1 - L^+ \leq z^+ \leq 1 \quad (3.14)$$

For $L = L_{hc}$ ie. $L^+ = 1$

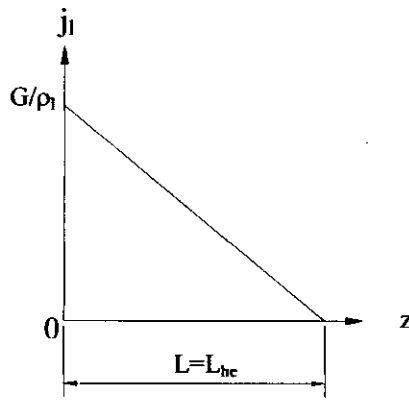


Fig. 3.5 Liquid velocity variation for $L=L_{hc}$

Here at $z=0$, $j_l = G/\rho_l$ as $\alpha=0$ (flow is in liquid phase only)

$$\therefore j_l = \frac{G(1-z^+)}{\rho_l} \quad \text{for } 0 \leq z^+ \leq 1 \quad (3.15)$$

$$Re_f = \frac{G \cdot D \cdot (1-z^+)}{\mu_l} \quad \text{for } 0 \leq z^+ \leq 1 \quad (3.16)$$

For $L < L_{hc}$, ie. $L^+ > 1$

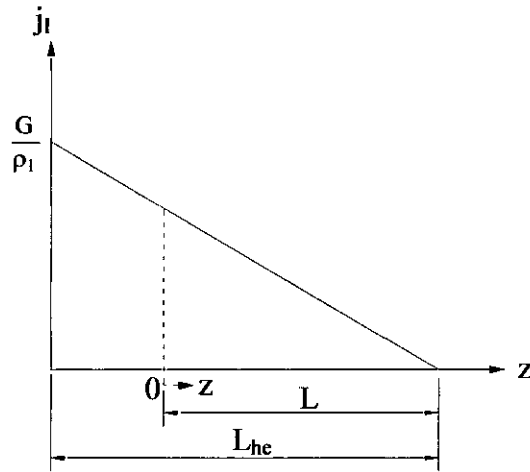


Fig. 3.6 Liquid velocity variation for $L < L_{hc}$

For $z = -(L_{hc}-L)$ to 0 , j_l decreases due to wall friction only because in this region $\alpha=0$ and $j_l = G/\rho_l L^+$ at $z=0$.

$$\therefore j_l = \frac{G(1-z^+)}{\rho_l L^+} \quad \text{for } 0 \leq z^+ \leq 1 \quad (3.17)$$

$$Re_f = \frac{G.D.(1-z^+)}{\mu_l L^+} \quad \text{for } 0 \leq z^+ \leq 1 \quad (3.18)$$

Now using the above relations of j_l and Re_f and the equation (3.9) we can get the expression of frictional force for various conditions as follows-

For $L > L_{hc}$ or $L^+ < 1$

$$F_w = \pi r_0 L \rho_l \int_0^1 C_{fw} \frac{j_l^2}{[1-(z^+)^{2/n}]^2} dz^+$$

Using Eqs. 3.9 and 3.10, we get,

$$F_w = \pi r_0 L \rho_l \left[\int_0^{1-L^+} C_{fw} \frac{G^2}{\rho_l^2 \{1-(z^+)^{2/n}\}^2 \{1-(z^+)^{2/n}\}^2} dz^+ + \int_{1-L^+}^1 C_{fw} \frac{G^2 (1-z^+)^2}{\rho_l^2 \{1-(1-L^+)^{2/n}\}^2 L^2 \{1-(z^+)^{2/n}\}^2} dz^+ \right]$$

$$\Rightarrow F_w = \frac{\pi r_0 G^2 L}{\rho_1} \left[\int_0^{1-L^+} \frac{C_{fw}}{\{1-(z^+)^{2/n}\}^4} dz^+ + \int_{1-L^+}^1 \frac{C_{fw} (1-z^+)^2}{\{1-(1-L^+)^{2/n}\}^2 L^{+2} \cdot \{1-(z^+)^{2/n}\}^2} dz^+ \right]$$

$$\Rightarrow F_w = \frac{\pi r_0 G^2 L}{\rho_1} I$$

Where,

$$I = \left[\int_0^{1-L^+} \frac{C_{fw}}{\{1-(z^+)^{2/n}\}^4} dz^+ + \int_{1-L^+}^1 \frac{C_{fw} (1-z^+)^2}{\{1-(1-L^+)^{2/n}\}^2 L^{+2} \cdot \{1-(z^+)^{2/n}\}^2} dz^+ \right]$$

Let $I = I_1 + I_2$

Here,

$$I_1 = \int_0^{1-L^+} \frac{C_{fw}}{\{1-(z^+)^{2/n}\}^4} dz^+$$

$$I_2 = \int_{1-L^+}^1 \frac{C_{fw} (1-z^+)^2}{\{1-(1-L^+)^{2/n}\}^2 L^{+2} \cdot \{1-(z^+)^{2/n}\}^2} dz^+$$

The Leibniz Integral rule

$$\frac{\partial}{\partial z} \int_{a(z)}^{b(z)} f(x, z) dx = \int_{a(z)}^{b(z)} \frac{\partial f}{\partial z} dx + f(b(z), z) \frac{\partial b}{\partial z} - f(a(z), z) \frac{\partial a}{\partial z}$$

$$\frac{\partial I_1}{\partial L} = \int_0^{1-L^+} \frac{\partial C_{fw}}{\partial L} \frac{dz^+}{\{1-(z^+)^{2/n}\}^4} + \frac{C_{fw}}{\{1-(1-L^+)^{2/n}\}^4} \frac{\partial(1-L^+)}{\partial L}$$

Let,

$$x = [1-(1-L^+)^{2/n}]^4$$

$$\therefore \frac{dx}{dL} = \frac{-2}{n} (1-L^+)^{\frac{2}{n}-1} \frac{L^{+2}}{L_{hc}}$$

Now,

$$\frac{\partial C_{fw}}{\partial L} = \frac{\partial C_{fw}}{\partial Re_1} \cdot \frac{\partial Re_1}{\partial L}$$

$$= \frac{\partial C_{fw}}{\partial Re_1} \cdot \frac{\partial}{\partial L} \left[\frac{GD}{[1-z^{+2/n}] \mu_1} \right]$$

$$\therefore \frac{\partial C_{fw}}{\partial L} = - \frac{\partial C_{fw}}{\partial \operatorname{Re}_1} \cdot \frac{2GD(z^+)^{\frac{2}{n}} L^+}{\mu_1 \left\{ 1 - (z^+)^{\frac{2}{n}} \right\}^2 L_{hc} n}$$

$$\therefore \frac{\partial I_1}{\partial L} = - \int_0^{1-L^+} \left[\frac{\partial C_{fw}}{\partial \operatorname{Re}_1} \cdot \frac{2GD(z^+)^{\frac{2}{n}} L^+}{\mu_1 \left\{ 1 - (z^+)^{\frac{2}{n}} \right\}^2 L_{hc} n} + C_{fw} \frac{\partial}{\partial L} \left\{ 1 - (z^+)^{\frac{2}{n}} \right\}^{-4} \right] dz^+ + \frac{C_{fw}}{x^4} \frac{\partial(1-L^+)}{\partial L}$$

$$\Rightarrow \frac{\partial I_1}{\partial L} = - \int_0^{1-L^+} \left[\frac{\partial C_{fw}}{\partial \operatorname{Re}_1} \cdot \frac{2GD(z^+)^{\frac{2}{n}} L^+}{\mu_1 \left\{ 1 - (z^+)^{\frac{2}{n}} \right\}^6 L_{hc} n} + \frac{C_{fw} 8(z^+)^{\frac{2}{n}} L^+}{\left\{ 1 - (z^+)^{\frac{2}{n}} \right\}^5 L_{hc} n} \right] dz^+ + \frac{C_{fw}}{x^4} \frac{\partial(1-L^+)}{\partial L}$$

$$\text{Let, } \frac{\partial C_{fw}}{\partial \operatorname{Re}_1} \cdot \frac{2GD(z^+)^{\frac{2}{n}} L^+}{\mu_1 \left\{ 1 - (z^+)^{\frac{2}{n}} \right\}^6 L_{hc} n} = P_4$$

$$\text{and, } \frac{C_{fw} 8(z^+)^{\frac{2}{n}} L^+}{\left\{ 1 - (z^+)^{\frac{2}{n}} \right\}^5 L_{hc} n} = P_5$$

$$\therefore \frac{\partial I_1}{\partial L} = - \int_0^{1-L^+} (P_4 + P_5) dz^+ + \frac{C_{fw}}{x^4} \cdot \frac{\partial(1-L^+)}{\partial L}$$

Now,

$$I_2 = \int_{1-L^+}^1 \frac{C_{fw} (1-z^+)^2}{\left\{ 1 - (1-L^+)^{2/n} \right\}^2 L^{+2} \cdot \left\{ 1 - (z^+)^{2/n} \right\}^2} dz^+$$

$$\Rightarrow I_2 = \int_{1-L^+}^1 \frac{C_{fw} (1-z^+)^2}{L^{+2} x^{+2} \cdot \left\{ 1 - (z^+)^{2/n} \right\}^2} dz^+$$

$$\therefore \frac{\partial I_2}{\partial L} = \int_{1-L^+}^1 \frac{\partial}{\partial L} \left[\frac{C_{fw}}{L^{+2} x^{+2}} \right] \cdot \frac{(1-z^+)^2}{\left\{ 1 - (z^+)^{2/n} \right\}^2} dz^+ - \frac{C_{fw}}{x^4} \frac{\partial(1-L^+)}{\partial L}$$

Here,

$$\frac{\partial}{\partial L} \left[\frac{C_{fw}}{L^{+2}x^2} \right] = \frac{L^{+2}x^2 \frac{\partial C_{fw}}{\partial L} - C_{fw} \left[L^{+2} \cdot 2x \cdot (-1) \cdot \frac{2(1-L^+)^{\frac{2}{n}-1} \cdot L^{+2}}{L_{he} \cdot n} + x^2 \cdot \left(-\frac{L^{+3}}{L_{he}} \right) \right]}{(L^{+2}x^2)^2}$$

$$\therefore \frac{\partial}{\partial L} \left[\frac{C_{fw}}{L^{+2}x^2} \right] = \frac{\partial C_{fw}}{\partial L} \cdot \frac{1}{L^{+2}x^2} + \frac{C_{fw}}{L_{he} \cdot x^3} \left[\frac{4(1-L^+)^{\frac{2}{n}-1}}{n} + \frac{x}{L^+} \right]$$

$$\text{Let, } \frac{C_{fw}}{L_{he} \cdot x^3} \left[\frac{4(1-L^+)^{\frac{2}{n}-1}}{n} + \frac{x}{L^+} \right] = P_3$$

And,

$$\frac{\partial}{\partial L} \left[(1-z^+)^2 / [1-(z^+)^{2/n}]^2 \right] = \frac{[1-(z^+)^{2/n}]^2 \cdot \frac{\partial}{\partial L} (1-z^+)^2 - (1-z^+)^2 \cdot \frac{\partial}{\partial L} [1-(z^+)^{2/n}]^2}{[1-(z^+)^{2/n}]^4}$$

$$= \frac{[2 \cdot \{1-(z^+)^{2/n}\}^2 \cdot (1-z^+) \cdot z^+ \cdot L^+ / L_{he}] - [4 \cdot (1-z^+)^2 \cdot \{1-(z^+)^{2/n}\} \cdot (z^+)^{2/n} L^+ / n \cdot L_{he}]}{[1-(z^+)^{2/n}]^4}$$

$$\therefore \frac{\partial}{\partial L} \left\{ (1-z^+)^2 / [1-(z^+)^{2/n}]^2 \right\} = \frac{2(1-z^+)z^+L^+}{[1-(z^+)^{2/n}]^2 \cdot L_{he}} - \frac{4(1-z^+)(z^+)^{\frac{2}{n}}L^+}{[1-(z^+)^{2/n}]^3 \cdot n \cdot L_{he}} = P_2$$

$$\begin{aligned} \therefore \frac{\partial I_2}{\partial L} &= \int_{1-L^+}^1 \left[\left[\left\{ \frac{\partial C_{fw}}{\partial L} \cdot \frac{1}{L^{+2}x^2} + \frac{C_{fw}}{L^{+2}x^2} \left(\frac{4(1-L^+)^{(2/n)-1}}{n} - \frac{x}{L^+} \right) \right\} \cdot \frac{(1-z^+)^2}{\{1-(z^+)^{2/n}\}^2} \right] \right. \\ &\quad + \left. \left[\frac{C_{fw}}{L^{+2}x^2} \left\{ \frac{2(1-z^+)z^+L^+}{\{1-(z^+)^{2/n}\}^2 L_{he}} - \frac{4(1-z^+)(z^+)^{\frac{2}{n}}L^+}{\{1-(z^+)^{2/n}\}^3 \cdot n \cdot L_{he}} \right\} \right. \right. \\ &\quad \left. \left. + \frac{C_{fw}}{L^{+2}x^2} \left(\frac{4(1-L^+)^{\frac{2}{n}-1}}{n} - \frac{x}{L^+} \right) \right] \right] dz^+ - \frac{C_{fw}}{x^4} \cdot \frac{\partial(1-L^+)}{\partial L} \end{aligned}$$

Again,

$$\frac{\partial C_{fw}}{\partial L} = \frac{\partial C_{fw}}{\partial Re_1} \cdot \frac{\partial Re_1}{\partial L}$$

$$\text{Here, } \frac{\partial Re_1}{\partial L} = \frac{\partial}{\partial L} \left\{ \frac{GD(1-z^+)}{[1-(1-L^+)^{2/n}]^2 \mu_1 L^+} \right\}$$

$$\Rightarrow \frac{\partial Re_1}{\partial L} = \frac{GD}{\mu_1} \left[\frac{1}{xL_{he}} + \frac{(1-z^+).2.(1-L^+)^{\frac{2}{n}-1} L^+}{xL_{he}.n} \right]$$

$$\therefore \frac{\partial C_{fw}}{\partial L} = \frac{\partial C_{fw}}{\partial Re_1} \cdot \frac{GD}{\mu_1} \left[\frac{1}{xL_{he}} + \frac{2.(1-z^+).(1-L^+)^{\frac{2}{n}-1} L^+}{xL_{he}.n} \right] = P_1$$

$$\therefore \frac{\partial I_2}{\partial L} = \int_{1-L^+}^1 \left[\left(\frac{P_1}{L^{+2}x^2} + P_3 \right) \cdot \frac{(1-z^+)^2}{[1-(z^+)^{2/n}]^2} + P_2 \cdot \frac{C_{fw}}{L^{+2}x^2} \right] dz^+ - \frac{C_{fw}}{x^4} \cdot \frac{\partial(1-L^+)}{\partial L}$$

Let,

$$\left(\frac{P_1}{L^{+2}x^2} + P_3 \right) \cdot \frac{(1-z^+)^2}{[1-(z^+)^{2/n}]^2} = P_6$$

$$P_2 \cdot \frac{C_{fw}}{L^{+2}x^2} = P_7$$

$$\therefore \frac{\partial I_2}{\partial L} = \int_{1-L^+}^1 (P_6 + P_7) dz^+ - \frac{C_{fw}}{x^4} \cdot \frac{\partial(1-L^+)}{\partial L}$$

$$\therefore \frac{\partial I}{\partial L} = - \int_0^{1-L^+} (P_4 + P_5) dz^+ + \int_{1-L^+}^1 (P_6 + P_7) dz^+$$

For $L=L_{he}$

$$F_w = \pi r_0 \rho_l L \int_0^1 C_{fw} \frac{j_l^2}{[1-(z^+)^{2/n}]^2} dz^+$$

$$j_l = \frac{G(1-z^+)}{\rho_l}$$

$$\therefore F_w = \pi r_0 \rho_l L \int_0^1 C_{fw} \frac{G^2 (1-z^+)^2}{[1-(z^+)^{2/n}]^2} dz^+$$

$$\Rightarrow F_w = \frac{\pi r_0 G^2 L}{\rho_l} I$$

Where,

$$I = \int_0^1 C_{fw} \frac{(1-z^+)^2}{[1-(z^+)^{2/n}]^2} dz^+$$

$$\therefore \frac{\partial I}{\partial L} = \frac{\partial}{\partial L} \int_0^1 C_{fw} \frac{(1-z^+)^2}{[1-(z^+)^{2/n}]^2} dz^+$$

Applying Leibniz Integral rule, we get

$$\frac{\partial I}{\partial L} = \int_0^1 \left[\frac{\partial C_{fw}}{\partial L} \cdot \frac{(1-z^+)^2}{[1-(z^+)^{2/n}]^2} + C_{fw} \frac{\partial}{\partial L} \frac{(1-z^+)^2}{[1-(z^+)^{2/n}]^2} dz^+ \right]$$

Now,

$$\frac{\partial C_{fw}}{\partial L} = \frac{\partial C_{fw}}{\partial Re_1} \cdot \frac{\partial Re_1}{\partial L}$$

$$\frac{\partial C_{fw}}{\partial L} = \frac{\partial C_{fw}}{\partial Re_1} \cdot \frac{GD}{\mu_l} \cdot \left(\frac{z^+ L^+}{L_{hc}} \right)$$

We have,

$$\frac{\partial}{\partial L} \left\{ \frac{(1-z^+)^2}{[1-(z^+)^{2/n}]^2} \right\} = P_2$$

$$\therefore \frac{\partial I}{\partial L} = \int_0^1 \left[\left\{ \frac{\partial C_{fw}}{\partial L} \cdot \frac{GD}{\mu_l} \cdot \left(\frac{z^+ L^+}{L_{hc}} \right) \cdot \frac{(1-z^+)^2}{[1-(z^+)^{2/n}]^2} \right\} + (C_{fw}) \cdot P_2 \right] dz^+$$

$$\text{Let, } \frac{\partial C_{fw}}{\partial L} \cdot \frac{GD}{\mu_l} \cdot \left(\frac{z^+ L^+}{L_{hc}} \right) \cdot \frac{(1-z^+)^2}{[1-(z^+)^{2/n}]^2} = P_8$$

$$\therefore \frac{\partial I}{\partial L} = \int_0^1 [(P_8) + (C_{fw} \cdot P_2)] dz^+$$

For, $L < L_{hc}$

$$F_w = \pi r_0 L \rho_1 \int_0^1 C_{fw} \frac{j_l^2}{[1 - (z^+)^{2/n}]^2} dz^+$$

We have, $j_l = \frac{G(1 - z^+)}{\rho_1 L^+}$

$$\therefore F_w = \pi r_0 \rho_1 L \int_0^1 C_{fw} \frac{G^2(1 - z^+)^2}{[1 - (z^+)^{2/n}]^2} dz^+$$

Where,

$$I = \int_0^1 C_{fw} \frac{(1 - z^+)^2}{L^{+2} [1 - (z^+)^{2/n}]^2} dz^+$$

$$\therefore \frac{\partial I}{\partial L} = \int_0^1 \left[\frac{\partial}{\partial L} \left(\frac{C_{fw}}{L^{+2}} \right) \left\{ \frac{(1 - z^+)^2}{[1 - (z^+)^{2/n}]^2} \right\} + \left\{ \frac{C_{fw}}{L^{+2}} \cdot \frac{(1 - 1)^2}{[1 - (1)^{2/n}]^2} \right\} \right] dz^+$$

Here,

$$\frac{\partial}{\partial L} \left(\frac{C_{fw}}{L^{+2}} \right) = \frac{2C_{fw}}{L^{+3}} \cdot \frac{\partial L^{+2}}{\partial L_{hc}} + \frac{1}{L^{+2}} \cdot \left(\frac{\partial C_{fw}}{\partial Re_1} \cdot \frac{\partial Re_1}{\partial L} \right)$$

We have,

$$Re_1 = \frac{GD(1 - z^2)}{\mu_1}$$

$$\therefore \frac{\partial Re_1}{\partial L} = \frac{GD}{\mu_1} \cdot \frac{\partial}{\partial L} \left(\frac{1 - z^+}{L^+} \right)$$

$$\therefore \frac{\partial}{\partial L} \left(\frac{C_{fw}}{L^{+2}} \right) = \frac{2C_{fw}}{L^+ L_{hc}} + \frac{1}{L^{+2}} \left(\frac{\partial C_{fw}}{\partial Re_1} \cdot \frac{GD}{\mu_1 L_{hc}} \right)$$

$$\text{Let, } \frac{2C_{fw}}{L^+ L_{hc}} + \frac{1}{L^{+2}} \left(\frac{\partial C_{fw}}{\partial Re_1} \cdot \frac{GD}{\mu_1 L_{hc}} \right) = q_1$$

$$\text{so, } \frac{\partial I}{\partial L} = \int_0^1 \left[q_1 \cdot \frac{(1 - z^+)^2}{[1 - (z^+)^{2/n}]^2} + \frac{C_{fw}}{L^{+2}} \cdot P_2 \right] dz^+$$

$$\text{Let, } q_1 \cdot \frac{(1 - z^+)^2}{[1 - (z^+)^{2/n}]^2} = q_2$$

$$\text{and, } \frac{C_{fw}}{L^{+2}} \cdot P_2 = q_3$$

$$\therefore \frac{\partial I}{\partial L} = \int_0^1 (q_2 + q_3) dz^+$$

Hence the frictional force becomes,

$$F_w = \frac{\pi r_0 G^2 L}{\rho_l} \cdot I$$

where,

$$I = \left[\int_0^{1-L^+} \frac{C_{fw}}{\{1-(z^+)^{2/n}\}^4} dz^+ + \int_{1-L^+}^1 \frac{C_{fw}(1-z^+)^2}{\{1-(1-L^+)^{2/n}\}^2 L^{+2} \cdot \{1-(z^+)^{2/n}\}^2} dz^+ \right], \quad \text{for } L^+ < 1$$

$$= \int_0^1 C_{fw} \frac{(1-z^+)^2}{[1-(z^+)^{2/n}]^2} dz^+, \quad \text{for } L^+ = 1$$

$$= \int_0^1 C_{fw} \frac{(1-z^+)^2}{L^{+2} [1-(z^+)^{2/n}]^2} dz^+, \quad \text{for } L^+ > 1$$

Using the value of F_P , F_G , F_w , and F_M in the equation (3.7), we get

$$\therefore F_1(G, L) = \frac{\pi r_0 G^2 L}{\rho_l} \cdot I + \left(\frac{k_v}{\rho_v} - \frac{k_l}{\rho_l} \right) r_0^2 \cdot G^2 + \pi r_0^2 g L (\rho_v - \rho_l) \frac{n}{n+2} + 2\pi r_0 \sigma = 0 \quad (3.19)$$

From the energy balance at a certain heat flux, q , we get

$$q = \frac{H_{lg} DG}{4L_{hc}} \quad (3.20)$$

At the CHF, q fixes the profile length, L maximizing the mass flux, G .

$$\text{So, for maximum } G, \quad \frac{\partial G}{\partial L} = 0$$

According to Euler's theorem, Eq. (3.19) can be written as-

$$\begin{aligned} \frac{\partial F_1}{\partial G} \partial G + \frac{\partial F_1}{\partial L} \partial L &= 0 \\ \Rightarrow \frac{\partial F_1}{\partial G} \cdot \frac{\partial G}{\partial L} + \frac{\partial F_1}{\partial L} &= 0 \end{aligned} \quad (3.21)$$

Hence, from Eq. (3.21), we get

$$\frac{\partial F_1}{\partial L} = 0 = F_2(G, L) \quad (\text{Let})$$

$$\Rightarrow F_2(G, L) = \frac{\pi r_0 G^2}{\rho_1} \left(L \frac{\partial I}{\partial L} + I \right) + \pi r_0^2 g (\rho_v - \rho_l) \frac{n}{n+2} = 0 \quad (3.22)$$

Solution of the simultaneous Eqs. (3.19) and (3.22) will result the maximum G and then using the Eq. (3.20) the value of CHF can be predicted as follows-

$$q_{co} = \frac{H_{lg} D G_{max}}{4L_{he}} \quad (3.23)$$

3.3 SOLUTION PROCEDURE

The relations above are closed now. Knowing the properties of fluid and geometric parameters, the above model can be solved as follows-

- (1) An initial guess is made for the mass flux, G and the profile length, L
- (2) Within the guess range of G and L, the value of the functions $F_1(G, L)$ and $F_2(G, L)$ from the Eqs. (3.19) and (3.22) are computed for a particular tube geometry, working fluid and working condition (Appendix B).
- (3) The contour of the functions $F_1(G, L)$ and $F_2(G, L)$ are plotted against the range of G and L (Appendix C).
- (4) The intersection point of the contour $F_1(G, L) = 0$ and $F_2(G, L) = 0$ is the solution of the Eqs. (3.19) and (3.22) and gives the maximum mass flux, G_{max} for a particular tube geometry and thermal-hydraulic condition of the working fluid.
- (5) The value of G_{max} is used to calculate q_{co} using the Eq. (3.23).

3.4 RANGES OF THE ANALYSIS

CHF data of natural convective boiling in vertical heated tube has been calculated by varying several parameters namely, working fluid, working pressure, tube diameter, and tube heating length, the profile index and heating length and diameter ratio. Different values of these parameters are categorically given in the Table 3.1 which is identical with the experimental ranges of Monde et al. [31]

Analysis are conducted for eight different density ratios in the range of $\rho_v/\rho_l = 6.22 \times 10^{-4} - 0.2095$, eleven different L_{hc}/D in the range of 5 to 857 and for working fluid R113, R12 and water.

Table 3.1 Ranges of the analysis

Working Fluid	Pressure (MPa)	Heating Length (mm)	Tube Diameter (mm)	L_{hc}/D	ρ_v/ρ_l	Profile index, n
R113	0.1-0.3	23-960	1.12-18.4	5-857	4.95×10^{-3} -0.0147	2-14
R12	0.793-2.907	23-960	1.12-18.4	5-857	0.0348-0.2095	2-4
Water	0.1	23-960	1.12-18.4	5-857	6.22×10^{-4}	2-4

3.5 CLOSURE

Analysis model, assumptions, methodology, and analysis ranges have been discussed in this chapter. In the following chapter, CHF data of this analytical study will be presented as functions of different parameters, and the characteristics of CHF will also be discussed.

RESULTS AND DISCUSSION

Critical heat flux (CHF) in the present analysis has been defined as the heat flux in annular flow regime, which leads to the wall temperature excursion of the heated tube and deterioration of heat transfer from the heating wall due to the termination of continuous liquid contact with the wall. The vapor, from the continuous vapor phase in the bulk flow, covers the heated surface. In this analysis around 300 CHF data, of which 33 for water, 99 for R113, and 165 for R12 are calculated by varying different parameters mentioned in Table 3.1 of the previous chapter. Thermo-physical properties of different working fluids necessary to calculate several variables used in this chapter are given in Table A.1 of Appendix A.

4.1 CHF CHARACTERISTICS

Many CHF data have been calculated by varying the tube geometry and thermal-hydraulic conditions of the various working fluids, which is done to evaluate the effects of various parameters on CHF and to compare these with existing CHF data of similar geometry and thermal-hydraulic conditions. Accordingly, Fig. 4.1 has been constructed with the present analytical data to explain the basic CHF characteristics of different working fluids and Fig. 4.2 representing the experimental data (Monde et al. [31]) has been constructed to compare the characteristics of CHF with the analytical ones.

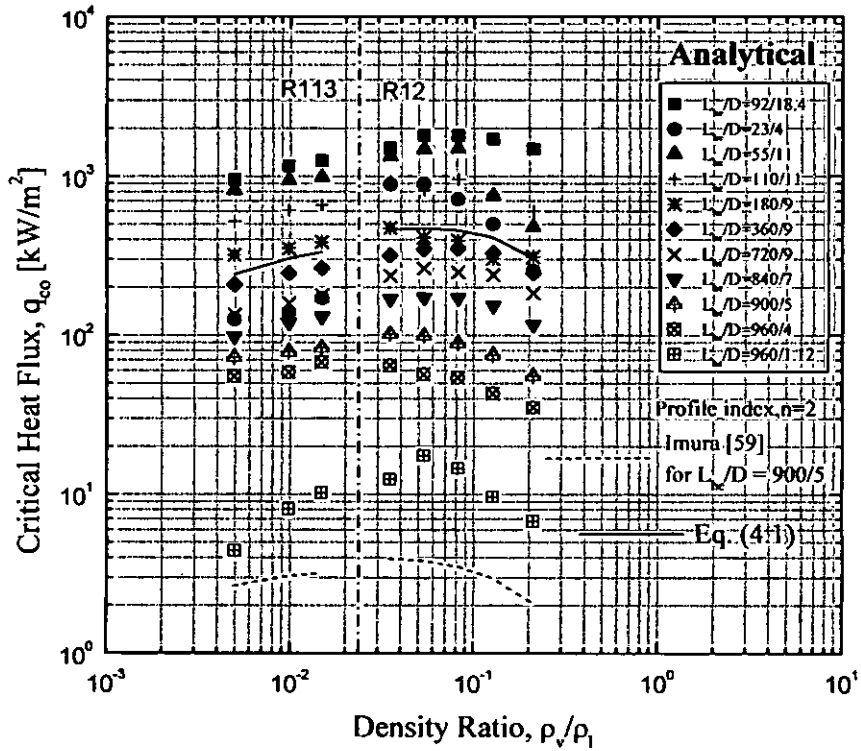


Fig. 4.1 Characteristics of the CHF in natural convective boiling of saturated liquid in vertical tubes (analytical)

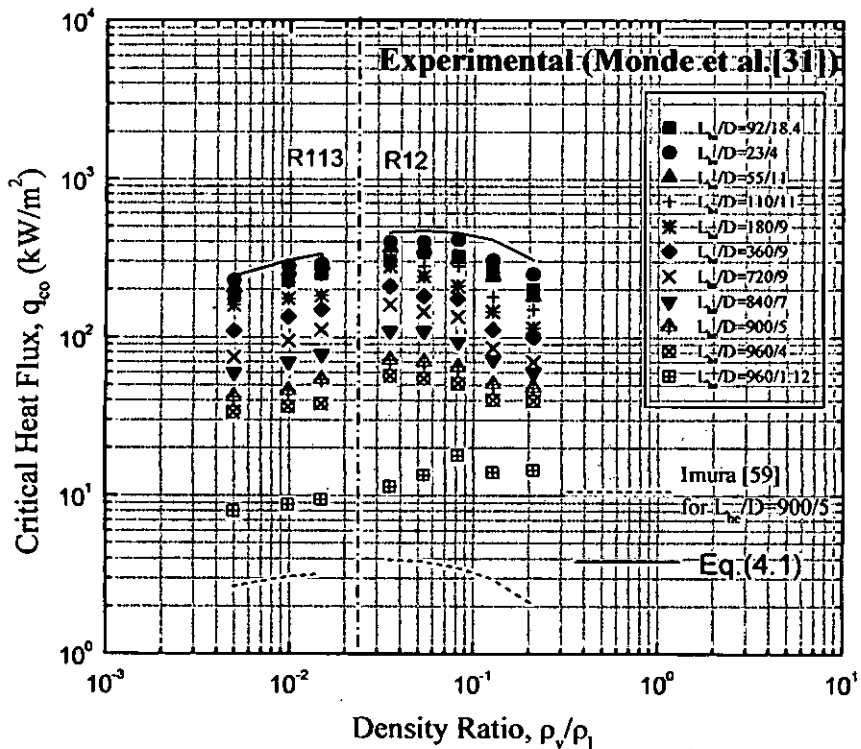


Fig. 4.2 Characteristics of the CHF of natural convective boiling of saturated liquid in vertical tubes (Experimental, Monde et al. [31])

Figure 4.1 represents all the CHF data plotted against the density ratio (ρ_v/ρ_l). The solid line for each working fluid as shown in this figure is the Kutateladze correlation, Eq. (4.1) for predicting the CHF in an ordinary saturated pool boiling.

$$Ku = \frac{q_{co} / \rho_v H_{lg}}{\sqrt[4]{\sigma g (\rho_l - \rho_v) / \rho_v^2}} = 0.16 \quad (4.1)$$

Where Ku is called the Kutateladze number for dimensionless CHF in saturated pool boiling.

Each of the symbols in Fig. 4.1 represents a CHF data for a particular combination of heating length and diameter of the vertical tube. The CHF in a vertical tube basically depends on the ratio L_{hc}/D and ρ_v/ρ_l and its character has a tendency similar to Kutateladze's prediction for saturated pool boiling. The CHF of the present analysis should be smaller than the Kutateladze's prediction by Eq. (4.1) because this analysis is done for the boiling in a narrow confine of a tube whereas Eq. (4.1) is for pool boiling. But the Fig. 4.1 shows that some of the CHF for smaller L_{hc}/D are higher than the Kutateladze's prediction and this may be due to the various assumptions that are considered for the simplification of this analysis. The dotted line for each working fluid in the Figs. 4.1 and 4.2 represents the Imura's correlation [59] for closed thermosyphon.

For the same value of L_{hc}/D , the CHF increases with an increase of ρ_v/ρ_l for R113, while decreases for R12. This is because of the working pressures chosen in this study such that the reduced pressure, P_r , is in the range of 0.192 to 0.703 for R12 and $P_r \ll 0.192$ for R113. It is well known that the CHF increases with P_r and becomes maximum at a working pressure of about $P_c/3$ (i.e. $P_r=1/3$), beyond which it decreases continuously [55]. As P_r increases with ρ_v/ρ_l , the CHF as shown in Fig. 4.1 is obtained. It is worth mentioning that for a constant ρ_v/ρ_l , the CHF increases with an increase in tube diameter for a fixed length of the tube and decreases with an increase in tube length for a constant tube diameter. These are also explained clearly in section 4.3-4.5. The Characteristics of the analytical CHF values in the Fig. 4.1 shows the similar tendency as in the Fig. 4.2, which was the prediction of CHF experimentally by Monde et al. [31]. The analytical model always overpredicts the CHF than the experimental model except for the $L_{hc}/D=23/4$ and $L_{hc}/D=960/1.12$ in case of R113

and at $L_{hc}/D=960/1.12$ for R12. Again for Water, Fig. 4.6 shows that the analytical model overpredicts the CHF for $L_{hc}/D = 960/4$.

4.2 EFFECTS OF PRESSURE ON CHF

Fig. 4.2 shows the CHF variation with eight different working pressures for two L_{hc}/D . Both analytical and experimental CHF values of R113 and R12 are shown here. For R113 CHF increases with the increase of pressure while for R12 it decreases and its reasons have already discussed in section 4.1. Pressure has a weak influence on the CHF for low-pressure range. The pressure change from 0.1 MPa to 0.3 MPa causes only 13 percent of CHF changes but it is significant in the high pressure region where the reduced pressure, P_r near to 1 (Bewilogua et al., [56]). Fig.4.2 also shows that the variations of CHF with pressure for both analytical model and experimental model have the same tendency.

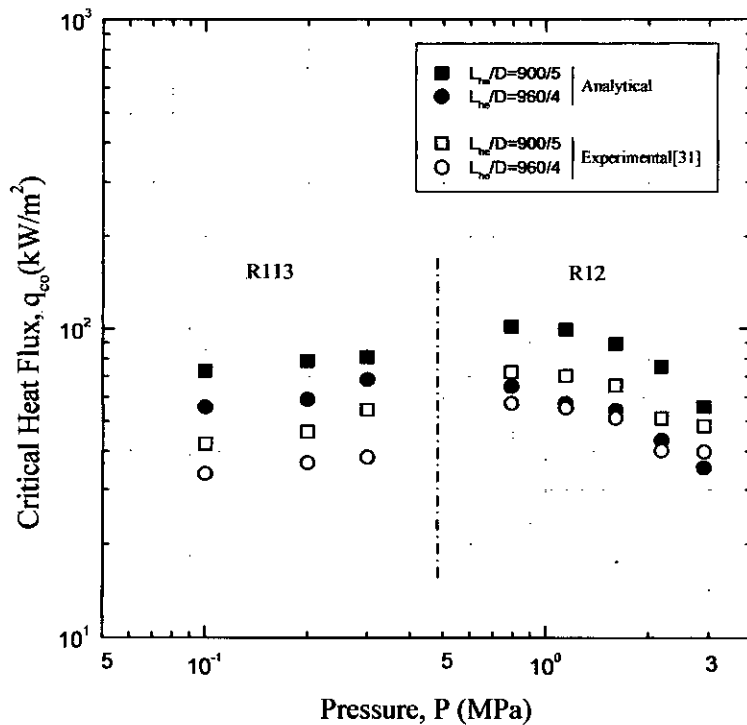


Fig. 4.3 Effect of working pressure, P on CHF

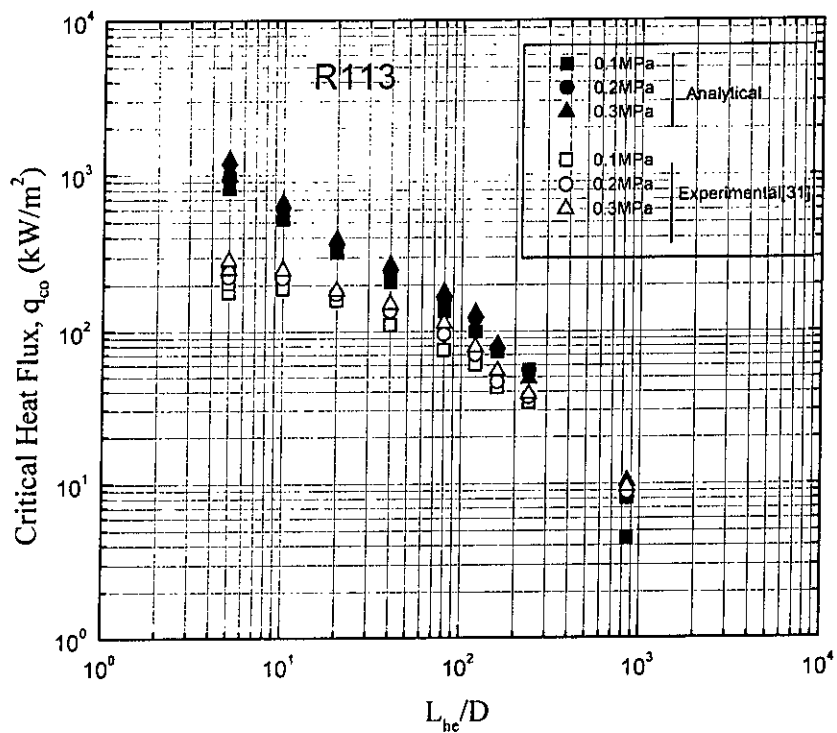


Fig. 4.4 Effect of L_{hc}/D on CHF for R113

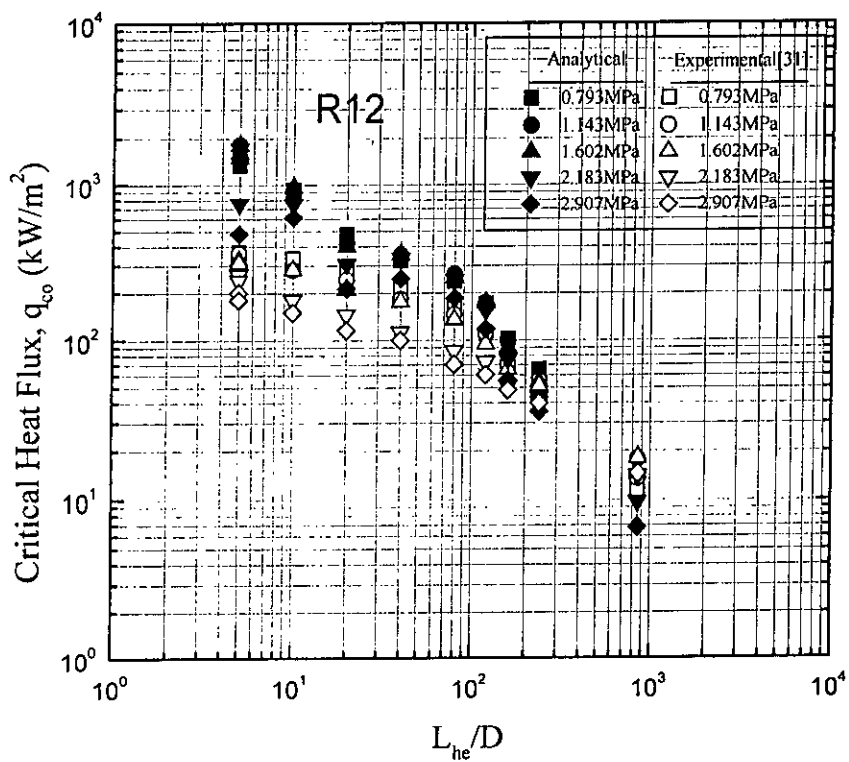


Fig. 4.5 Effect of L_{hc}/D on CHF for R12

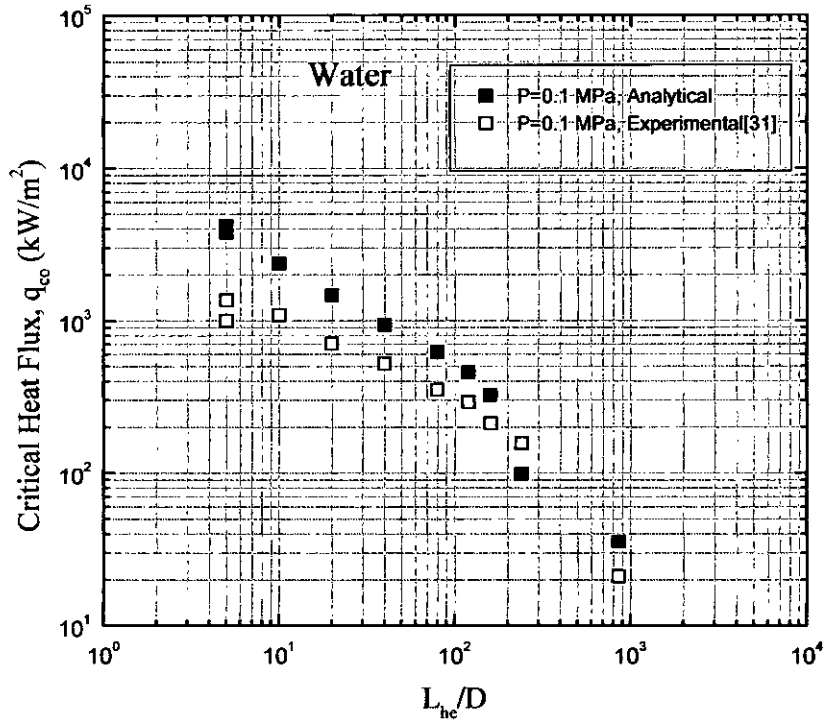


Fig. 4.6 Effect of L_{he}/D on CHF for Water

4.3 EFFECTS OF L_{he}/D ON CHF

Influences of tube heating length and diameter ratio, L_{he}/D on CHF are shown in the Figs. 4.4, 4.5 and 4.6 where different symbols are for different working pressures. For all the working fluid, CHF decreases as the L_{he}/D increases and the changes are more significant for $L_{he}/D < 50$. In this range an increase of L_{he}/D by 10 decreases 22% of the CHF while above this range it decreases only 4%. Therefore, the effect of L_{he}/D on CHF is less significant for $L_{he}/D > 50$.

4.4 EFFECTS OF TUBE HEATING LENGTH, L_{he} ON CHF

The variations of CHF with the tube heating length, L_{he} for a fixed diameter, $D = 9\text{mm}$, are depicted in Figs. 4.7 and 4.8. The CHF for both R113 and R12 decreases as the heating length, L_{he} increases but the changes become more flat at higher L_{he} than the lower L_{he} region.

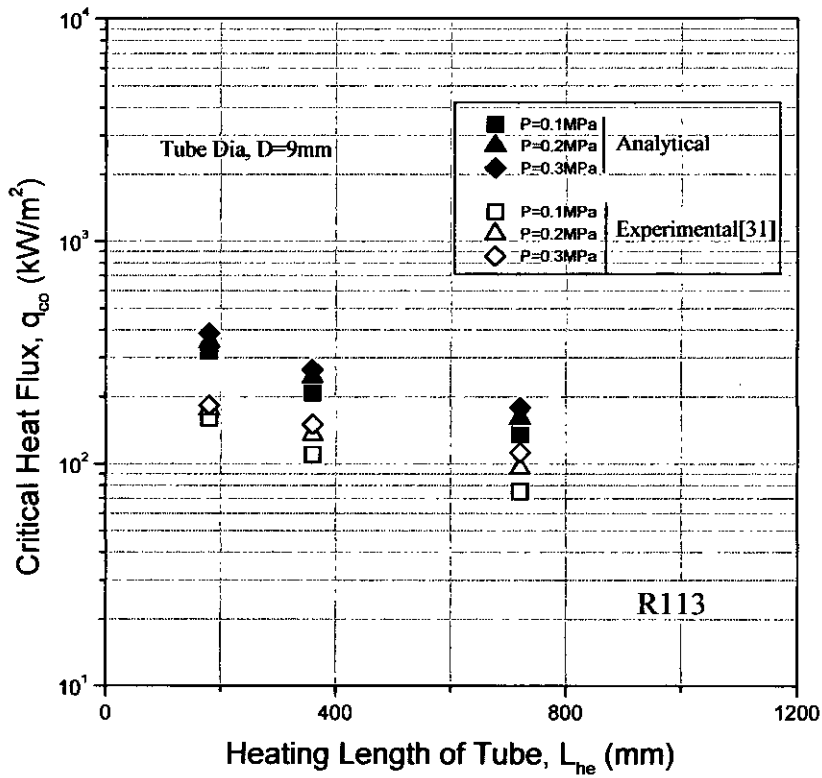


Fig. 4.7 Effect of tube heating length, L_{he} on CHF for R113

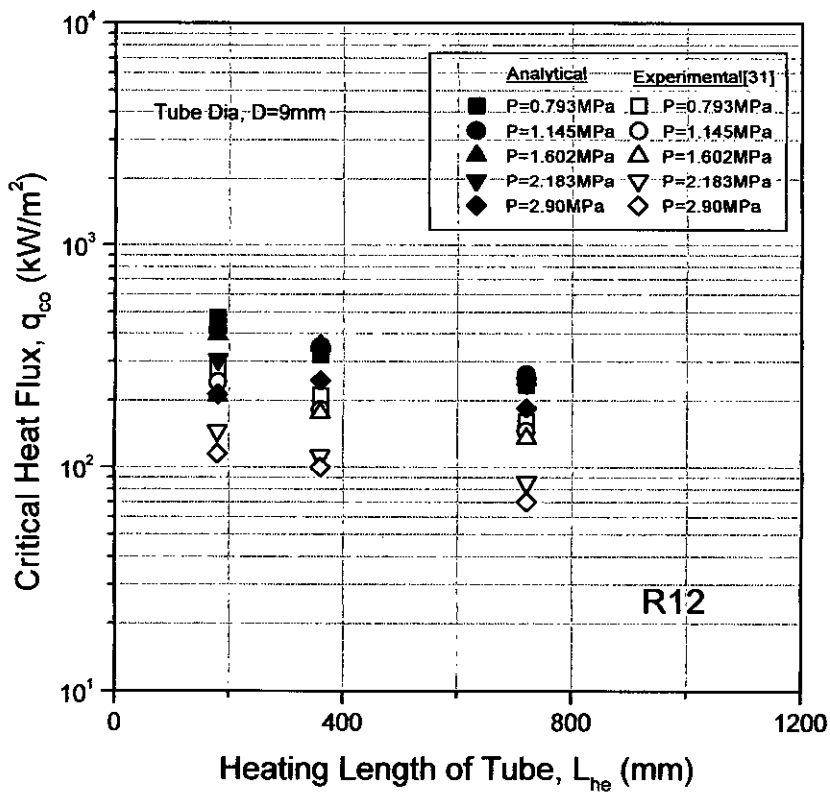


Fig. 4.8 Effect of tube heating length, L_{he} on CHF for R12

4.5 EFFECTS OF TUBE DIAMETER, D ON CHF

Figures 4.9 and 4.10 show the CHF variation with tube diameter, D for $L_{he} = 960$ mm, where different symbols are for different working pressures. For a constant heating length of the tube, the CHF for both the working fluids increases with the increase of tube diameter because the boiling characteristics shift towards the pool boiling for larger diameter.

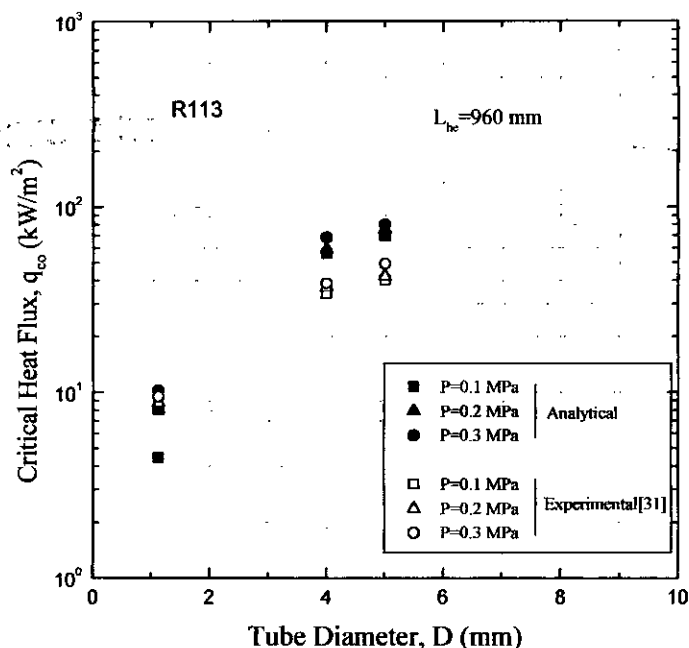


Fig. 4.9 Effect of tube diameter, D on CHF for R113

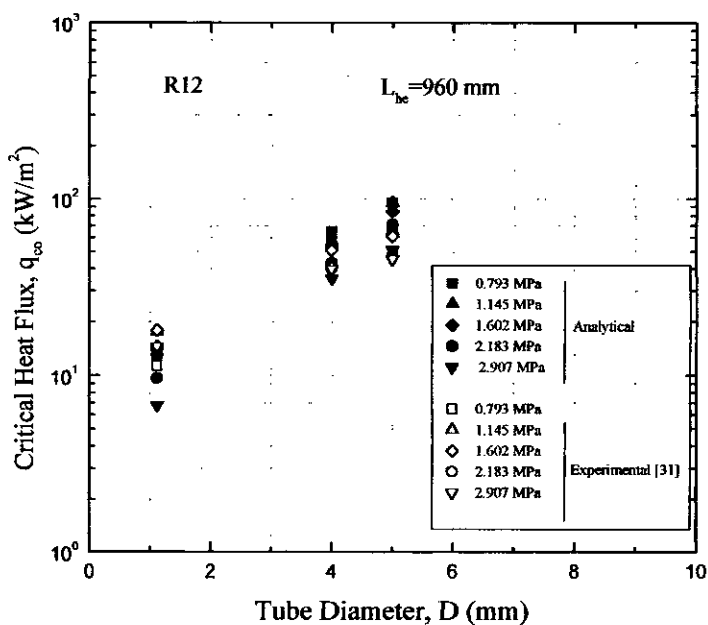


Fig. 4.10 Effect of tube diameter, D on CHF for R12

4.6 EFFECTS OF PROFILE INDEX, n ON CHF

The liquid-vapor interface of the annular flow in this analysis is assumed to be a smooth curve defined by Eq. (3.1) and Fig. 4.11 shows the change of the shape of the interface with the change of profile index, n . According to the Eq. (3.2) it also shows that for a fixed value of z and L , where $z \leq L$, the void fraction increases with the increase of n because the interface shape becomes wider at that z location for higher n . Fig. 4.12 shows the variation of CHF with the profile index n for the working fluid R113 at a fixed L_{he}/D . It shows that with the increase of n the CHF decreases because the void fraction increases with the n . At higher n the analytical CHF approaches to the experimental values but Fig. 4.13 shows that the change of the CHF is significant upto $n = 8$ and then further increase of n has very little effect on CHF. The effect of n on CHF for R12 and Water may have the same characteristics as shown for R113 and one may use higher n , upto 8, for better results of the present analysis.

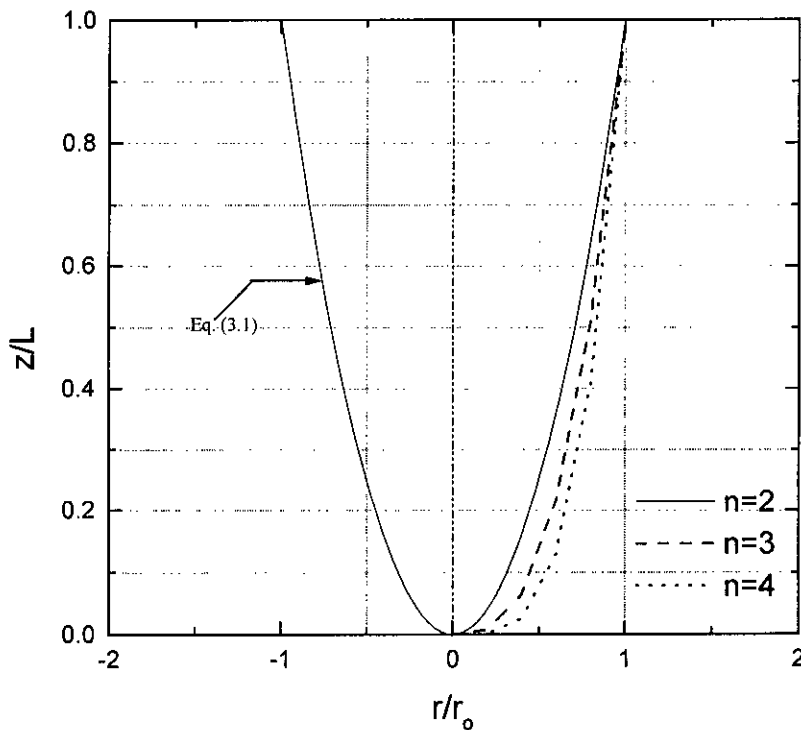


Fig. 4.11 Effects of profile index ' n ' on the liquid-vapor interface shape

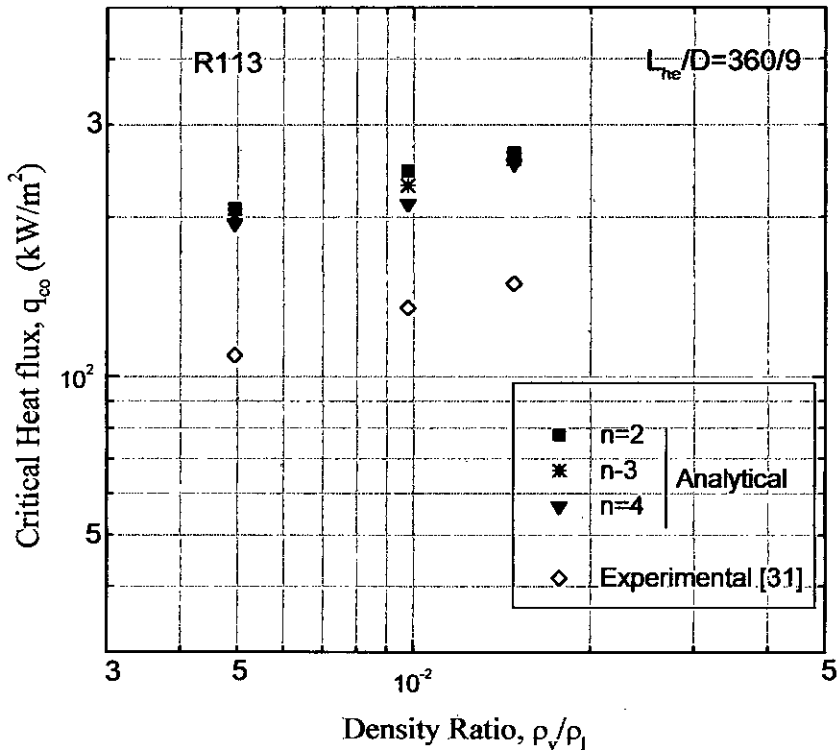


Fig. 4.12 Effect of profile index 'n' on CHF at different pressure

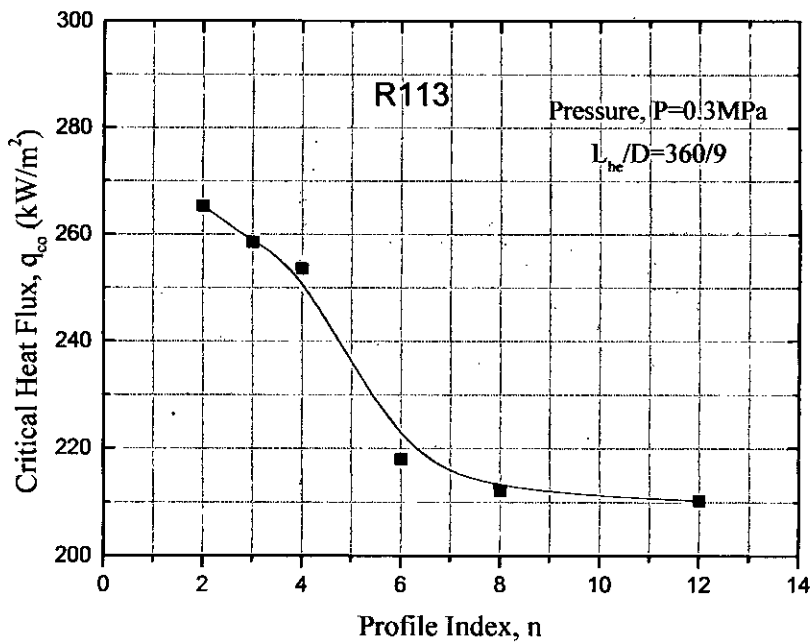


Fig. 4.13 Effect of profile index, n on CHF

4.7 EFFECTS OF WORKING FLUIDS ON CHF

In this analysis CHF data have been calculated for different working fluids, viz. Water, R113 and R12 at different pressures to study the effect of physical properties of the fluids on the CHF. A comparison is made in Fig. 4.14 for water at $P=0.1\text{MPa}$, R113 at $P=0.1\text{MPa}$ and R12 at $P=0.793\text{MPa}$ by varying the L_{hc}/D . The operating conditions are not identical but a qualitative comparison can easily be made from this figure. The CHF for R113 is the smallest of that for the liquids used in the present study for a particular L_{hc}/D . This is due to the smallest heat of vaporization of R113.

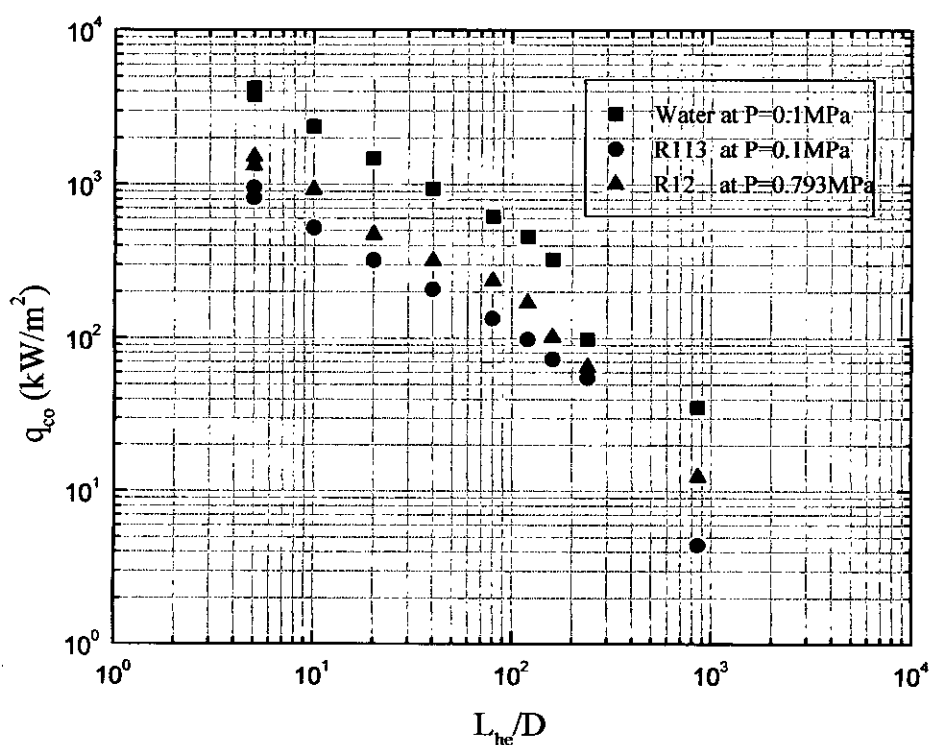


Fig. 4.14 Effect of working fluid on CHF

4.8 VERIFICATION OF THE PRESENT MODEL

To test the basic performance of the present analytical model, the CHF data of R113, R12 and Water of this analysis have compared with the experimental data that were measured by Monde et al. [31] at the same geometry and thermal-hydraulic conditions given in the table 3.1. The comparison has done with the help of Kutateladze correlation (4.1). Figures 4.15, 4.16 and 4.17 show the comparison of reciprocal of Kutateladze number for experimental model with that of the present analytical model. Though these figures for R113, R12 and water indicate that the present model has the tendency to over-and under-predict the experimental CHF values, the analytical CHF

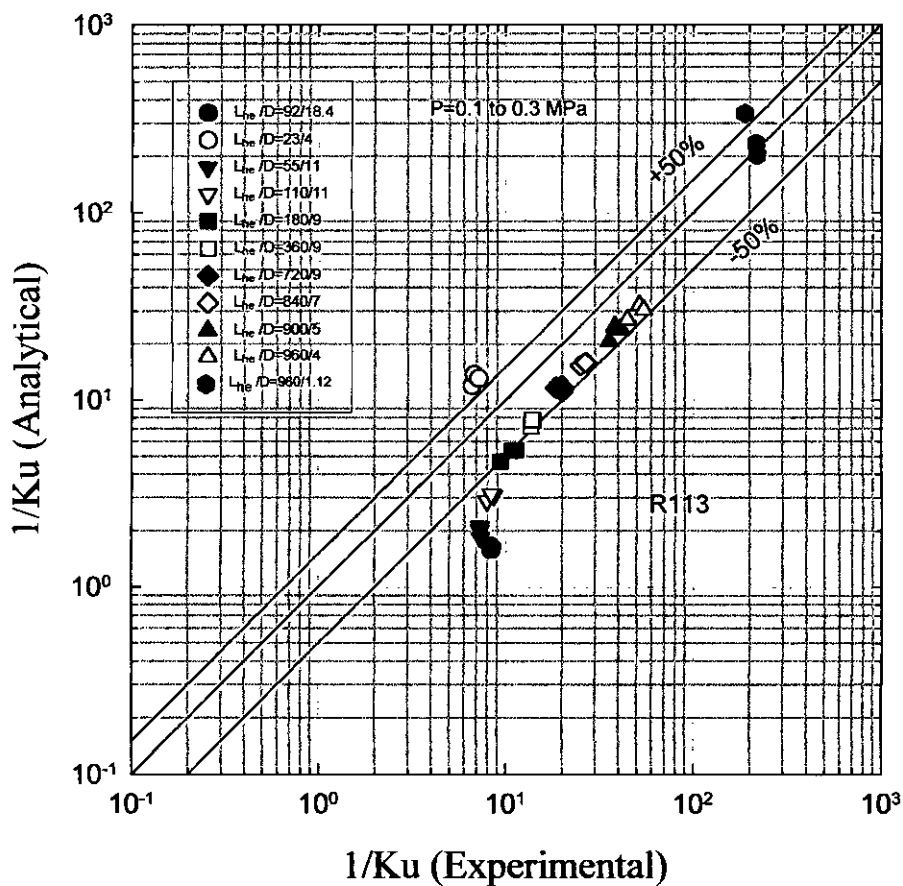


Fig. 4.15 Comparison between analytical and experimental CHF for R113

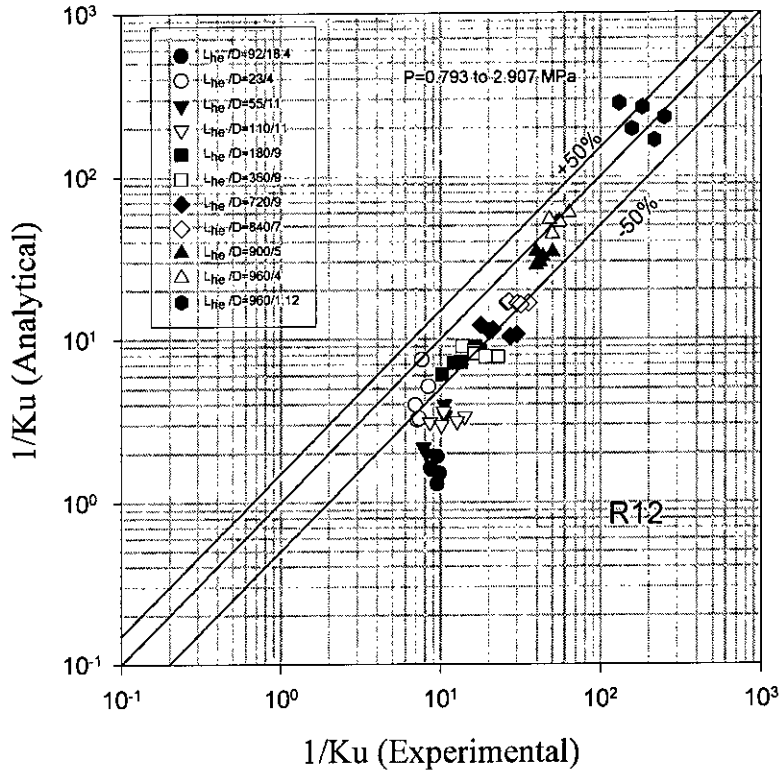


Fig. 4.16 Comparison between analytical and experimental CHF for R12

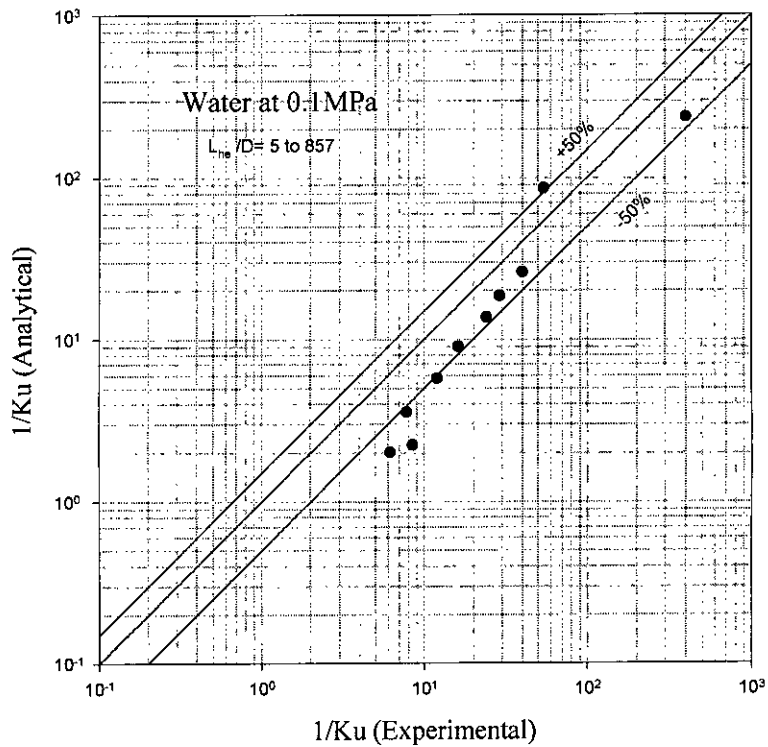


Fig. 4.17 Comparison between analytical and experimental CHF for water

values agree with the experimental CHF within $\pm 50\%$. Also the ratios between experimental and analytical critical heat fluxes, $q_{co}(\text{experimental})/q_{co}(\text{analytical})$ are plotted against L_{he}/D in Fig 4.18. It shows that the present model predicts the CHF well within $\pm 50\%$ for $L_{he}/D > 20$ and within $\pm 30\%$ for higher L_{he}/D but the significant scattering is seen in case of small L_{he}/D . For shorter L_{he}/D , the CHF characteristics are presumably similar to that of pool boiling giving its higher values as observed for both the present and existing experimental study. But the analytical values are much more higher than the experimental values because here $L \gg L_{hc}$ for maximum mass flux. This may be due to the absence of the tube wall (Fig. 3.3) for $z = 0$ to $(L - L_{he})$, which causes the in flow of excess liquid into the main flow with less friction. For $L_{he}/D > 20$, the present analysis shows some discrepancies as shown in Figs 4.15, 4.16 and 4.17, which may be attributed to the assumptions adopted in the present model.

Acceleration of the vapor core during vaporization process very often produces entrainment of the liquid droplet. This effect, together with direct vaporization of the film, tends to reduce the film thickness quickly than with no entrainment resulting in the decrease in CHF. But the present model did not consider entrainment and thus over-predicts the CHF.

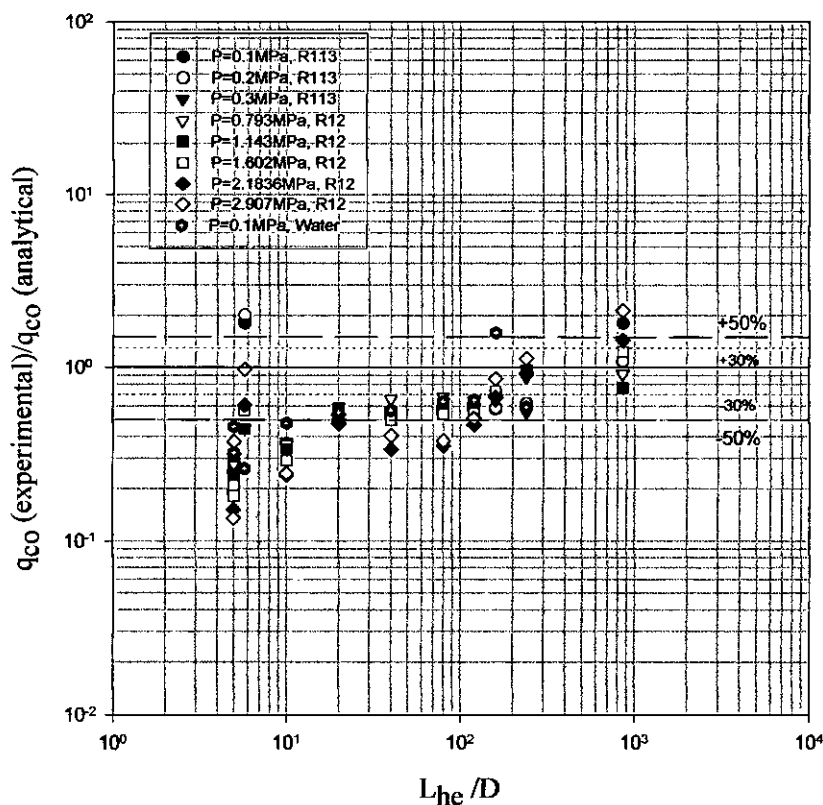


Fig. 4.18 Dependence of the present model on L_{he}/D

Phase-change systems are almost always subjected to instability associated with the liquid-vapor interface. This kind of instability of interface has strong impact on heat and mass transfer during phase change process, which is not considered in the present model. This may also be one of the reasons of over-predicting CHF by this model.

4.9 CLOSURE

An attempt has been made in this chapter to explain the CHF characteristics of the present model. The effects of various parameters on the CHF are also discussed here. In the following chapter a summary of the present work will be presented and conclusion will be drawn accordingly.

CONCLUSIONS

5.1 CONCLUSIONS

An analytical study has been made for the critical heat flux of natural convective boiling of saturated liquid in a vertical tube, where liquid and vapor form a co-current annular flow. Saturated Water, R113 and R12 at different pressures are the working fluids in this study to obtain CHF data for wide range of ρ_v/ρ_l (0.622×10^{-4} to 0.2095) and of L_{he}/D (5 to 857). The CHF data have been presented to show the effects of different parameters and are analyzed with a view to understanding its inherent characteristics. From the predicted CHF data presentation and subsequent analysis, following inferences may be drawn:

1. This model considers mass, momentum, and energy balances for the two-phase flow in a vertical tube submerged in a saturated liquid, where the liquid-vapor interface is a paraboloid formed by $z/L = (r/r_0)^n$. The CHF is assumed to be taken place at the exit of the heated tube when the void fraction is unity and the mass flux, G is maximum.
2. The predicted CHF values show the similar characteristics as shown in available experimental studies.
3. The liquid-vapor interface profile index, n has significant effect on CHF for R113, the recommended range of n is about 2-8.
4. The variations of the CHF with the L_{he}/D are more significant for $L_{he}/D < 50$.
5. The predicted CHF data agreed well with the experimental values within $\pm 50\%$ for $L_{he}/D > 20$.

5.2 RECOMMENDATIONS

In order to improve the prediction of CHF by this model, following suggestions may be taken into account.

1. A numerical method could be undertaken to solve the simultaneous equations developed for finding maximum mass flux, G_{\max} instead of the present graphical method.
2. The mass transfer due to entrainment and deposition of the liquid droplets between the liquid and vapor phases could be incorporated in this model.
3. Instability associated with the liquid-vapor interface can also be taken into account in this model rather than assuming the interface as a smooth curve because instability of the interface has strong impact on heat and mass transfer during phase change process.
4. This model could be employed to predict CHF in a concentric tube open thermosyphon as the flow situation is similar to the present system.
5. The effects of channel orientation, surface roughness and surface tension on the CHF may be incorporated for further investigations.

REFERENCES

1. Lang, C., 1888, *Transactions of Institute of Engineers and Shipbuilders*, Scotland, Vol. 32, pp. 279- 295.
2. Nukiyama, S., 1934, "Maximum and Minimum Values of Heat Transmitted from a Metal to Boiling Water Under Atmospheric Pressure," *Japanese Society of Mechanical Engineers*, Japan, Vol. 37, 367-373, S53-43.
3. Drew, T.B., and Mueller, A.C., 1937, "Boiling," *Transactions of AIChE*, Vol. 33, pp. 449-471.
4. Zuber, N., 1959, "Hydrodynamic Aspects of Boiling Heat Transfer," *Ph.D. thesis*, Research Laboratory, Los Angeles and Ramo-Wooldridge Corporation, University of California, Los Angeles.
5. Boyd, R.D., 1983, "Subcooled Flow Boiling Critical Heat Flux (CHF) and its Application to Fusion Energy Components. Part I. A Review of Fundamentals of CHF and Related Data Base," *Fusion Technology*, Vol. 7, pp. 7-30.
6. Boyd, R.D., 1983, "Subcooled Flow Boiling Critical Heat Flux (CHF) and its Application to Fusion Energy Components. Part II. A Review of Micro-convective, Experimental, and Correlational Aspects," *Fusion Technology*, Vol. 7, pp. 31-51.
7. Kutateladze, S.S., 1952, "Heat Transfer in Condensation and Boiling," USAEC Rep.tr-3370.

8. Katto, Y., & Kurosaka, T., 1979, "Critical Heat Flux of Natural Convection Boiling In Vertical Annular Channels," *Proc. 15th Natl. Heat Transfer Symposium of Japan*, pp.280-282.
9. Monde, M., Mihara, S. and Inoue, T., 1993, "An analytical Study of the Critical Heat Flux of a Two-Phase Thermosyphon," *Heat Transfer-Japanese Research*, 22(6), pp. 611-623
10. Kodama, S. and Kataoka, I., 2003, "Critical Heat Flux Prediction Method Based on Two-Phase Turbulence Model," *Journal of Nuclear Science and Technology*, Vol. 40, No. 10, pp. 725-733.
11. Collier, J.G., 1981, "Convective Boiling and Condensation," 2nd ed., *McGraw-Hill*, New York.
12. Carey, V.P., 1992, "Liquid-Vapor Phase-Change Phenomena," *Taylor & Francis*, USA.
13. Bergles, A. E., 1985, "Burnout in boiling heat transfer: High-quality forced-convection systems, in Two-Phase Flow and Heat Transfer," *China-U.S. Progress*, X.-j. Chen and T. N. Veziroglu, Eds., Hemisphere, New York, pp. 177-206.
14. Thompson, B., and Macbeth, R. V., 1964, "Boiling water heat transfer-Burnout in uniformly heated round tubes: A compilation of world data with accurate correlations," *Br. Report AEEW-R356*, Winfrith, U. K.
15. Doroshchuk, V. E, and Lantsman, F. P., 1970, "Selecting magnitudes of critical heat fluxes with water boiling in vertical uniformly heated tubes," *Thermal Eng. (USSR)*, English transl., vol. 17, no. 12, pp. 18-21.
16. Heat and Mass Transfer Section, Scientific Council, USSR Academy of Sciences, 1976, "Tabular data for calculating burnout when boiling water uniformly heated round tubes," *Thermal Eng. (USSR)*, English transl., vol. 23, no. 9, pp. 90-92.

17. Groenveld, D.C., Leung, L.K.H., Kirillov, P.L., Bobkov, V.P., Smogalev, I.P., Vinogradov, V.N., Huang, X.C., Royer, E., 1996, "The 1995 Lookup Table for Critical Heat Flux in Tubes," *Nuclear Engineering and Design*, Vol. 163, pp. 1-23.
18. Nariyai, H., and Inasaka, F., 1992, "Critical Heat Flux and Flow Characteristics of Subcooled Flow Boiling with Water in Narrow Tubes," *Dynamics of Two-Phase Flows*, CRC Press, pp. 689-708.
19. Celata, G.P., and Mariani, 1999, "CHF and Post-CHF (Post-Dryout) Heat Transfer," *Chapter 17, Handbook of Phase Change, Boiling and Condensation*, Edited by Kandlikar, S.G., Shoji, M., and Dhir, V.K., Taylor and Francis, New York, pp. 443-493.
20. Celata, G.P., 1992, "Subcooled Water Flow Boiling CHF with Very High Heat Fluxes," *Revue Generale De Thermique Fr.*, ISSN 0035-3159/106/9, pp. 106-114.
21. Celata, G.P., 1997, "Modelling of Critical Heat Flux in Subcooled Flow Boiling," *Keynote Lecture, Convective Flow and pool Boiling Conference*, Irsee, 18-23 May, pp. 33-44.
22. Tong, L.S., and Tang, Y.S., 1997, "Flow Boiling Crisis," *Chapter 5, Boiling Heat Transfer and Two-Phase Flow*, Taylor and Francis, New York.
23. Bowring, R. W., 1972, "A simple but accurate round tube uniform heat flux dryout correlation over the pressure range 0.7-17 MN/m² (100-2500 psia)," *Br. Report AEEW-R789*, Winfrith, U. K.
24. Baisi, L., Clerici, G.C., Gariloben, S., Sala, R., and Tozzi, A., 1967, "Studies on burnout, Part 3, A new correlation for round ducts and uniform heating and its comparison with world data," *Energia Nucleare*, vol. 14, no. 9, pp. 530-536.

25. Katto, Y., and Ohno, H., 1984, "An improved version of the generalized correlation of critical heat flux for the forced convective boiling in uniformly heat vertical tubes," *Int. J. Heat Mass Transfer*, vol. 27, pp. 1641-1648.
26. Katto, Y., 1978, "A generalized correlation of critical heat flux for the forced convective boiling in vertical uniformly heated round tubes," *Int. J. Heat Mass Transfer*, vol. 21, pp. 1527-1542.
27. Katto, Y., 1979, "A generalized correlation of critical heat flux for the forced convective boiling in vertical uniformly heated round tubes—A supplementary report," *Int. J. Heat Mass Transfer*, vol. 22, pp. 783-794.
28. Shah, M. M., 1979, "A generalized graphical method for predicting CHF in uniformly heated vertical tubes," *Int. J. Heat Mass Transfer*, vol. 22, pp. 557-568.
29. Levy, S., Healzer, J. M., and Abdollahian, D., 1980, "Prediction of critical heat flux for annular flow in vertical pipes," *EPRI Report no. NP-1619*.
30. Greoneveld, D. C., Kiameh, B.P., and Chang, S. C., 1986, "Prediction of critical heat flux(CHF) for non-aqueous fluids in forced convective boiling," *Proc. 8th Int. Heat Transfer Conf.*, Hemisphere, New York, vol. 5, pp. 2209-2214.
31. Monde, M., and Yamaji, K., 1990, "Critical Heat Flux During Natural Convective Boiling in Vertical Uniformly Heated Tubes Submerged in Saturated Liquid," *Heat Transfer 1990, Proc. of 9th Heat Transfer, Conf.*, Jerusalem, Israel.
32. Kutateladze, S.S., Leontev, A.I., 1966, "Some Applications of the Asymptotic Theory of the Turbulent Boundary Layer," *Proceedings of the 3rd International Heat Transfer Conference*, Vol. 6, pp. 2373-2378.
33. Mattson, R.J., Hammitt, F.G., and Tong, L.S., 1973, "A Photographic Study of the Subcooled Flow Boiling Crisis in Freon-113," *Paper No. HT-39, ASME*, 8 pages.

34. Tong, L.S., Efferding, L.E., and Bishop, A.A., 1966, "A Photographic Study of Subcooled Boiling and DNB of Freon-113 in a Vertical Channel," *ASME Paper 66-WA/HT-39*, ASME Winter Annual Meeting, ASME, New York.
35. Fiori, M.P., and Bergles, A.E., 1970, "Model of Critical Heat Flux in Subcooled Flow Boiling," *Proceedings of the 4th International Heat Transfer Conference*, Vol. VI, paper B6.3.
36. Kirby, D.B., Staniforth, J.R., Kinneir, J.H., 1965, "A Visual Study of Forced Convection Boiling, Part I Results for a Flat Vertical Heater," *UK Rep. AEEW-R-281*, UK AEEW, Winfrith, England.
37. Bergel'son, B.R., 1980, "Burnout under Conditions of Subcooled Boiling and Forced Convection," *Thermal Engineering*, Vol. 27, No. 1, pp. 48-50.
38. Hebel, W., Detavernier, A., and Decreton, M., 1981, "A Contribution to the Hydrodynamics of Boiling Crisis in a Forced Flow of Water," *Nuclear Engineering and Design*, Vol. 64, pp. 433-445.
39. Weisman, J., and Pei, B.S., 1983, "Prediction of Critical Heat Flux in Flow Boiling at Low Qualities," *International Journal of Heat and Mass Transfer*, Vol. 26, No. 10, pp. 1463-1477.
40. Katto, Y., and Yokoya, 1970, "Principal Mechanism of Boiling Crisis in Pool Boiling," *International Journal of Heat and Mass Transfer*, Vol. 11, pp. 993-1002.
41. Haramura, Y., and Katto, Y., 1983, "A New Hydrodynamic Model of Critical Heat Flux, Applicable Widely to Both Pool and Forced Convection Boiling on Submerged Bodies in Saturated Liquids," *International Journal of Heat and Mass Transfer*, Vol. 26, pp. 379-399.

42. Haramura, Y., 1999, "Critical Heat Flux in Pool Boiling," *Chapter 6, Handbook of Phase Change: Boiling and Condensation*, Edited by S.G. Kandlikar, V.K. Dhir, and Shoji, M., Taylor and Francis, New York.
43. Katto, Y., 1990, "A Physical Approach to Critical Heat Flux of Subcooled Flow Boiling in Round Tubes," *International Journal of Heat and Mass Transfer*, Vol. 33, No. 3, 611-620.
44. Katto, Y., 1990b, "Prediction of Critical Heat Flux of Subcooled Flow Boiling in Round Tubes," *International Journal of Heat and Mass Transfer*, Vol. 33, No. 9, pp. 1921- 1928.
45. Lee, C.H., and Mudawar, I., 1988, "A Mechanistic Critical Heat Flux Model for Subcooled Flow Boiling Based on Local Bulk Flow Conditions," *International Journal of Multiphase Flow*, Vol. 14, No. 6, pp. 711-728.
46. Celata, G.P., Cumo, M., Mariani, A., Simoncini, M., and Zummo, G., 1994, "Rationalization of Existing Mechanistic Models for the Prediction of Water Subcooled Flow Boiling Critical Heat Flux," *International Journal of Heat and Mass Transfer*, Vol. 37, Supplement 1, pp. 347-360.
47. Whalley, P. B., Hutchinson, P., and Hewitt, G. F., 1974, "The calculation of critical heat flux in forced convective boiling," *Proc. 5th Int. Heat Transfer Conf.*, Tokyo, Paper B6. 11.
48. Whalley, P. B., 1976, "The calculation of dryout in rod bundle," *Br. Report AERE-R8319*.
49. Whalley, P. B., Hutchinson, P., and Hewitt, G. F., 1974, "Prediction of annular flow parameters for transient flows and for complex geometries," *Br. Report AERE-M2661*.

50. Govan, A. M., Hewitt, G. F., Owen, D. G., and Bott, T. R., 1988, "An improved CHF modeling code," *Proc. 2nd U.K. Conf. Heat Transfer, Institute of Mechanical Engineers, London*, vol. 1, pp. 33-48.
51. Hewitt, G. F. and Hall- Taylor, N. S., 1970, "Annular Two-Phase Flow," *Pergamon Press, Oxford*, chap. 11.
52. Hewitt, G. F., 1978, "Critical heat flux of boiling, Keynote lecture," *Proc. 6th Int. Heat Transfer Conf.*, Toronto, vol. 6, pp. 143-172.
53. Hewitt, G. F., 1982, "Burnout," in *Handbook of Multiphase System*, G. Hetsroni, Ed., *Hemisphere*, new York, sec. 6.4.
54. Okawa, T., Kotani, A., Katako, I., and Naito, M., 2003, "Prediction of Critical Heat Flux in Annular Flow Using a Film Flow Model," *Journal of Nuclear Science and Technology*, Vol. 40, NO. 6, pp. 388-396.
55. Stephan, K., 1987, "Heat Transfer in Condensation and Boiling," pp.160-161, *Springer-Verlag*.
56. Bewilogua, L., Knöner, and Vinzelberg, H., 1975, "Heat Transfer in Cryogenic Liquids under Pressure," *Cryogenics*, Vol. 15, No. 3, pp. 121-125.
57. Monde, M., 1996, "Analytical study of critical heat flux in two-phase thermosyphon: relationship between maximum falling liquid rate and critical heat flux," *Trans. ASME, J, Heat Transfer*, 118, pp.422-428.
58. Wallis, G. B., 1969, "One Dimensional Two-Phase Flow," p. 339, *McGraw- Hill*, New York.
59. Imura, H., Sasaguchi, K., Kozai, H., and Numata, S., 1983, "Critical Heat Flux in a Closed Two-Phase Thermosyphon," *Int. J. Heat Mass Transfer*, 26, pp. 1181-1188.

APPENDICES

- APPENDIX A** Thermo-Physical Properties of Working Fluid
- APPENDIX B** Flowchart and Program Code
- APPENDIX C** Analytical and Experimental Data Sample

APPENDIX A

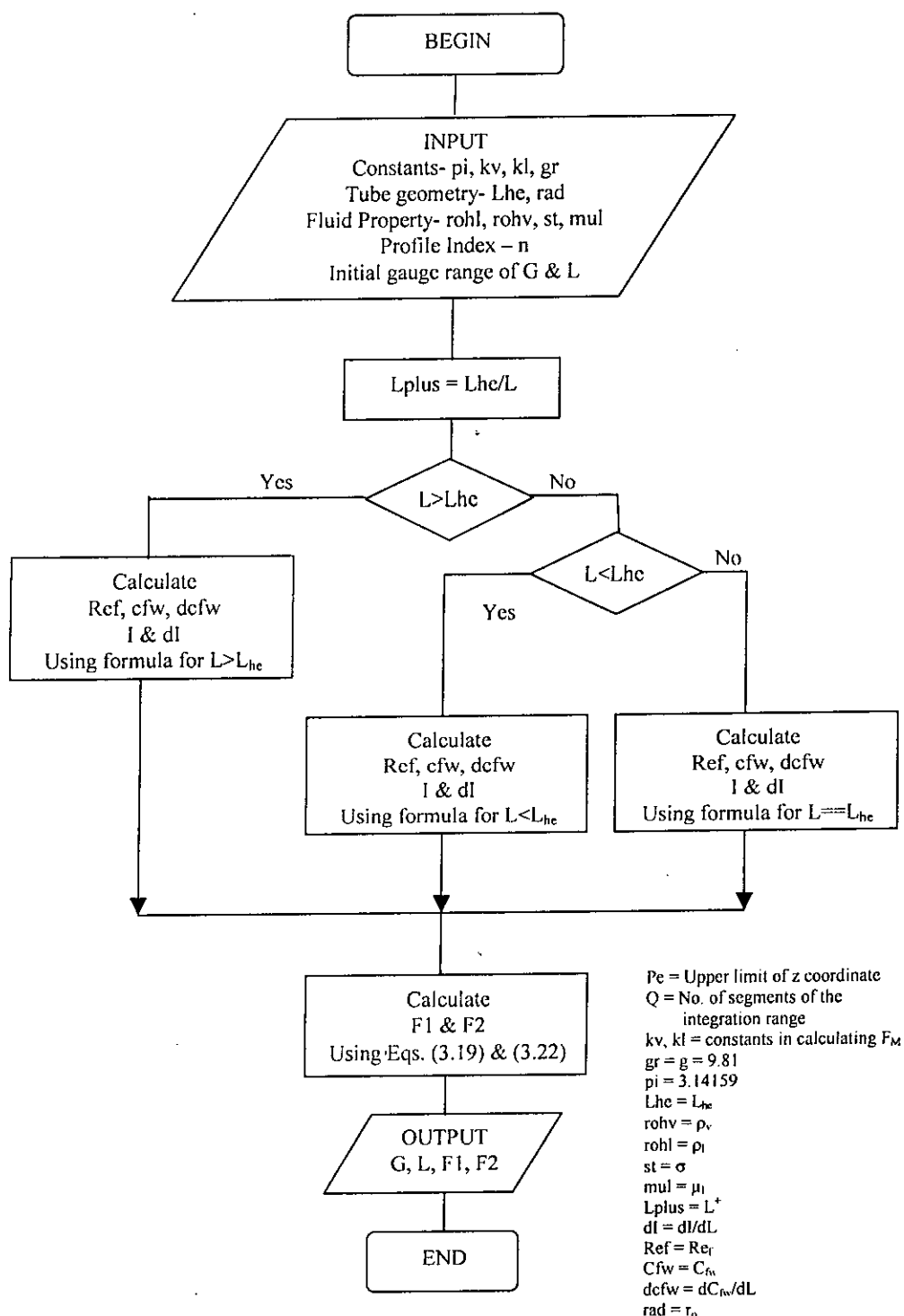
Thermo-Physical Properties of Working Fluids

Table A.1 Thermo-physical properties of working fluids [12]

Fluid	Thermo-Physical Properties						
	P [MPa]	T _{sat} [°C]	ρ _l [kg/m ³]	ρ _v [kg/m ³]	H _{lg} [kJ/Kg]	σ [mN/m]	μ _l [μNs/m ²]
Water	0.1	100	958.3	0.597	2257.8	58.98	284.62
R113	0.1	47.6	1507.6	7.457	143.8	14.66	494.07
	0.2	69.6	1452.2	14.177	138.9	12.31	385.67
	0.3	84.6	1412.5	20.885	130.7	10.75	329.94
R12	0.793	32	1284	44.8	137.7	7.7	208
	1.145	47	1225	65.4	127.2	5.9	187
	1.602	62	1157	94.6	114	4.2	167
	2.183	77	1057	136.4	97.6	2.8	144
	2.907	92	969.7	203.2	75.8	1.3	119

APPENDIX B

FLOW CHART OF THE COMPUTER PROGRAM



COMPUTER PROGRAM

```

% This is a Program to calculate F1 and F2 according to Eqs. (3.19) & (3.22).
% The Software used here is MATLAB 6.1

% Input the Constants
pi=3.14159; %  $\pi$ 
kv=3.2057; % constant required to calculate  $F_M$ 
kl=3.7399; % constant required to calculate  $F_M$ 
gr=9.81; % Gravitational acceleration ( $m/s^2$ )
Q=30.0; % No. of segments of the total range of integration required in
        % Simpson rule
Pe=0.9999; % Upper limit of the  $z^+ (= z/L)$  co-ordinate

% Input the tube geometry
rad=0.002; %  $r_o$  (m)
Lhe=0.023; %  $L_{he}$  (m)
n=2.0; % Liquid-Vapor interface profile index

% Input the fluid properties
rohv=6.33; %  $\rho_v$  ( $kg/m^3$ )
rohl=1486; %  $\rho_l$  ( $kg/m^3$ )
st=0.0155; %  $\sigma$  (N/m)
mul=0.000373; %  $\mu_l$  (Pa.s)
%.....
D=rad*2.0; %Tube diameter (m)

% Open output files for G, L, F1, F2
fidG = fopen('finalG.table','w');
fidL = fopen('finalL.table','w');
fidF1 = fopen('finalF1.table','w');
fidF2 = fopen('finalF2.table','w');
fidall = fopen('finalall.table','w');
%.....
for G=1:0.99:100 % For-loop for initial guess of G
    for L=0.001:0.001:1 % For-loop for initial guess of L

```

```

    Lplus=Lhe/L;          % L+
% Calculation of I & dI for L>Lhe
    if L>Lhe
        h=(1-Lplus)/Q;          % Length of each segment used for integration
        k=0;
        for zplus=0.0:h:(1-Lplus)    % z+
            Ref=(G*D)/((1.0-(zplus^(2.0/n)))*mul);    % Ref
            if Ref<160
                cfw=16/Ref;          % Cfw
                dcfw=-(16/(Ref^2));    % dCfw/dL
            elseif (Ref>=160) & (Ref<=10000)
                cfw=exp(5.48616-2.10284*log(Ref)+0.11855*((log(Ref))^2)-...
                0.130035*((log(Ref))^3));
                dcfw=cfw*((-2.10284/Ref)+(0.2371*log(Ref)/Ref)-(0.00390105*((...
                log(Ref))^2)/Ref));
            else
                cfw=0.079/(Ref^(1/4));
                dcfw=-0.01975/(Ref^(3/4));
            end
            k=k+1;
            F1(k)=cfw/((1.0-(zplus^(2.0/n)))^4.0);
            dF1(k)=((dcfw*2.0*G*D*(zplus^(2.0/n))*Lplus)/(mul*n*Lhe*((1.0-...
            (zplus^(2.0/n))^6.0)))+(cfw*8.0*(zplus^(2.0/n))*Lplus)/...
            (n*Lhe*((1.0-(zplus^(2.0/n)))^5.0)));
            end
        Isum1=0.0;
        dsum1=0.0;
        for j =2:1:Q
            Isum1=Isum1+2.0*F1(j);
            dsum1=dsum1+2.0*dF1(j);
        end
        Int1=(h/2.0)*(F1(1)+Isum1+F1(Q+1));
        dInt1=(h/2.0)*(dF1(1)+dsum1+dF1(Q+1));
    end

```

```

h2=(Pe-(1-Lplus))/Q;
k1=0;
for zplus =(1-Lplus):h2:Pe
Ref=(G*D*(1-zplus)/(((1-((1-Lplus)^(2/n)))^2)*(Lplus^2)*((1-...
zplus^(2/n))^2));
if Ref<160
    cfw=16/Ref;
    dcfw=-(16/(Ref^2));
elseif (Ref>=160) & (Ref<=10000)
    cfw=exp(5.48616-2.10284*log(Ref)+0.11855*((log(Ref))^2)-...
0.130035*((log(Ref))^3));
    dcfw=cfw*((-2.10284/Ref)+(0.2371*log(Ref)/Ref)-(0.00390105*((...
log(Ref))^2)/Ref));
else
    cfw=0.079/(Ref^(1/4));
    dcfw=-0.01975/(Ref^(3/4));
    end
k1=k1+1;
R=(1-(1-Lplus)^(2/n));
S=(1-(zplus^(2/n)));
F2(k1)=cfw*((1-zplus)^2)/((R^2)*(Lplus^2)*(S^2));
p1p1(k1)=((dcfw*G*D)/mul)*((1/R*Lhe)+(2*(1-zplus)*((1-Lplus)^(2/...
n)-1))*Lplus/(R^2)*Lhe^n));
p3p3(k1)=(cfw/Lhe*(R^3))*((4*((1-Lplus)^(2/n)-1)/n)+(R/Lplus));
p6p6(k1)=((p1p1(k1)/(Lplus^2)*(R^2))+p3p3(k1))*((1-zplus)^2)/(S^2);
p2p2(k1)=((2*(1-zplus)*zplus*Lplus/Lhe*(S^2))-((4*((1-zplus)^2)*...
(zplus^(2/n))*Lplus)/n*Lhe*(S^3)));
p7p7(k1)=(cfw/(Lplus^2)*(R^2))*p2p2(k1);
dF2(k1)=p6p6(k1)+p7p7(k1);
end
Isum2=0;
dsum2=0;
for j1 =2:1:Q
Isum2=Isum2+2*F2(j1);

```

```

dsum2=dsum2+2*dF2(j1);
end
Int2=(h2/2)*(F2(1)+Isum2+F2(Q+1));
dInt2=(h2/2)*(dF2(1)+dsum2+dF2(Q+1));
I=Int1+Int2;
dI=dInt2-dInt1;

```

% Calculation of I & dI for L=Lhe

```

elseif L==Lhe
h3=Pe/Q;
k2=0;
for zplus =0.0:h3:Pe
Ref=G*D*(1-zplus)/mul;
if Ref<160
cfw=16/Ref;
dcfw=-(16/(Ref^2));
elseif (Ref>=160) & (Ref<=10000)
cfw=exp(5.48616-2.10284*log(Ref)+0.11855*((log(Ref))^2)-...
0.130035*((log(Ref))^3));
dcfw=cfw*((-2.10284/Ref)+(0.2371*log(Ref)/Ref)-(0.00390105*((...
log(Ref))^2)/Ref));
else
cfw=0.079/(Ref^(1/4));
dcfw=-0.01975/(Ref^(3/4));
end
k2=k2+1;
H=(1-(zplus^(2/n)));
F3(k2)=cfw*((1-zplus)^2)/(H^2);
p8p8(k2)=dcfw*G*D*zplus*Lplus*((1-zplus)^2)/mul*Lhe*((1-(zplus^...
(2/n))^2);
p9p9(k2)=(2*(1-zplus)*zplus*Lplus/Lhe*(H^2))-((4*((1-zplus...
)^2)*(zplus^(2/n))*Lplus)/(n*Lhe*(H^3)));
dF3(k2)=p8p8(k2)+cfw*p9p9(k2);
end

```

```

Isum3=0;
dsum3=0;
for j2 =2:1:Q
Isum3=Isum3+2*F3(j2);
dsum3=dsum3+2*dF3(j2);
end
I=(h3/2)*(F3(1)+Isum3+F3(Q+1));
dI=(h3/2)*(dF3(1)+dsum3+dF3(Q+1));
% Calculation of I & dI for L<Lhe
else
h4=Pe/Q;
k3=0;
for zplus =0.0:h4:Pe
Ref=G*D*(1-zplus)/mul*Lplus;
if Ref<160
cfw=16/Ref;
dcfw=-(16/(Ref^2));
elseif (Ref>=160) & (Ref<=10000)
cfw=exp(5.48616-2.10284*log(Ref)+0.11855*((log(Ref))^2)-...
0.130035*((log(Ref))^3));
dcfw=cfw*((-2.10284/Ref)+(0.2371*log(Ref)/Ref)-(0.00390105*((...
log(Ref))^2)/Ref));
else
cfw=0.079/(Ref^(1/4));
dcfw=-0.01975/(Ref^(3/4));
end
k3=k3+1;
w=(1-(zplus^(2/n)));
F4(k3)=cfw*((1-zplus)^2)/(Lplus^2)*(w^2);
q1q1(k3)=(2*cfw/Lplus*Lhe)+(1/(Lplus^2))*(dcfw*G*D/mul*Lhe);
q2q2(k3)=q1q1(k3)*((1-zplus)^2)/w^2;
p10p10(k3)=((2*(1-zplus)*zplus*Lplus/Lhe*(w^2))-((4*((1-zplus)^2 ...
)*(zplus^(2/n))*Lplus)/n*Lhe*(w^3)));

```



```

q3q3(k3)=(cfw/(Lplus^2))*p10p10(k3);
dF4(k3)=q2q2(k3)+q3q3(k3);
end
Isum4=0;
dsum4=0;
for j3 =2:1:Q
Isum4=Isum4+2*F4(j3);
dsum4=dsum4+2*dF4(j3);
end
I=(h4/2)*(F4(1)+Isum4+F4(Q+1));
dI=(h4/2)*(dF4(1)+dsum4+dF4(Q+1));
end
% Calculation of F1 & F2
% Here F1=FF1 & F2=FF2
x=(pi*rad*G*G)/rohl;
y=pi*rad*rad*gr*(rohv-rohl)*(n/(n+2));
FF1=((x*I*L)+(y*L)+(((kv/rohv)-(kl/rohl))*rad*rad*G*G)-(2*pi*rad*...
st));
FF2=x*(L*dI+I)+y;
% Show output in the output file
fprintf(fidall,'%10.4f %10.4f %10.4f %10.4f\n',G,L,FF1,FF2)
fprintf(fidG,'%10.4f\n',G);
fprintf(fidL,'%10.4f\n',L);
fprintf(fidF1,'%10.4f\n',FF1);
fprintf(fidF2,'%10.4f\n',FF2);
end
end
fclose(fidall);
fclose(fidG);
fclose(fidL);
fclose(fidF1);
fclose(fidF2);

```

APPENDIX C

Analytical and Experimental Data sample

Table C.1 Analytical and experimental CHF data for R113 at n=2

L_{he} [mm]	D [mm]	L_{he}/D	P=0.1MPa		P=0.2MPa		P=0.3MPa	
			q_{co} [Ana]	q_{co} [Exp.]	q_{co} [Ana.]	q_{co} [Exp.]	q_{co} [Ana.]	q_{co} [Exp.]
92	18.4	5	954.048	180.2	1164.3	224.2	1253.5	250
23	4	5.75	126.36	228	138.85	280.3	159.57	289.3
55	11	5	819.02	205	942.59	260.2	983.69	284.1
110	11	10	520.18	190	614.14	221	660.82	248
180	9	20	321.56	160	352.54	175.2	386.04	183.2
360	9	40	208.39	110	245.42	135.3	265.4	150.2
720	9	80	134.88	75.1	159.43	95.2	178.17	112.2
840	7	120	98.48	60.03	120.53	70.1	131.15	78.1
900	5	160	72.74	42.2	78.5	46.2	83.2	54.2
960	4	240	55.58	33.7	58.8	36.6	68.3	38.2
960	1.12	857	4.44	8.02	8.09	8.8	10.24	9.5

Table C.2 Analytical and experimental CHF data for R12 at n=2

L_{he} [mm]	D [mm]	L_{he}/D	P=0.793MPa		P=1.145MPa		P=1.602MPa		P=2.183MPa		P=2.907MPa	
			q_{co} [Ana]	q_{co} [Exp.]	q_{co} [Ana.]	q_{co} [Exp.]	q_{co} [Ana.]	q_{co} [Exp.]	q_{co} [Ana]	q_{co} [Exp.]	q_{co} [Ana.]	q_{co} [Exp.]
92	18.4	5	1502.8	300.5	1807.6	340.2	1797	326	1708	260	1475.4	200.5
23	4	5.75	894.87	400.05	898.91	400.1	718	410	500.73	305.5	255.8	250.2
55	11	5	1325.4	366.2	1472.8	360.2	1482	310	754.83	240.2	478.98	180.4
110	11	10	925.34	333.2	817.89	280.5	960.16	280.2	746.08	180.2	609.35	150.2
180	9	20	472.96	280.2	414.19	242.2	395.58	210.2	304.43	145.02	213.18	115.4
360	9	40	319.65	210.1	349.95	182.5	351.88	175.5	330.68	112.3	245.84	100.12
720	9	80	235.59	160.5	263.81	145.6	249.37	135.2	239.53	85.5	184.87	70.3
840	7	120	170.33	110	173.49	110.2	172.49	94.2	154.23	72.4	117.25	60.3
900	5	160	101.6	72.2	99.26	70.02	89.165	65.2	75.23	51	55.63	48.2
960	4	240	64.92	57.2	57.18	55.2	54.36	51.2	43.31	40.2	35.24	39.8
960	1.12	857	12.43	11.36	17.65	13.5	14.58	18.01	9.67	14	6.788	14.5

Table C.3 Analytical and experimental CHF data for Water at $n=2$

L_{he} [mm]	D [mm]	L_{he}/D	P=0.1MPa	
			q_{co} [Ana]	q_{co} [Exp.]
92	18.4	5	4199.4	1364.085
23	4	5.75	3786.3	994.9799
55	11	5	2374.6	1084.273
110	11	10	1467.5	704.7774
180	9	20	937.95	522.0573
360	9	40	617.56	352.3887
720	9	80	456.49	291.632
840	7	120	324.96	211.4332
900	5	160	98.4	156.6172
960	4	240	35.53	21.12748
960	1.12	857	4199.4	1364.085

SAMPLE PROGRAM OUTPUT

For R113, n=2, Lhe= 840mm, D= 7mm, Lhe/D=120, P=0.3Mpa, $\rho_l=1412.5 \text{ kg/m}^3$,
 $\rho_v=20.885 \text{ kg/m}^3$, $\rho_v/\rho_l=14.78 \times 10^{-3}$

G	L	F1	F2
1.0000	0.1000	-0.0265	-0.2629
1.0000	0.6000	-0.1578	-1.5458
1.0000	1.1000	-0.2835	-3.9437
1.0000	1.6000	-0.4166	-0.3591
1.0000	2.1000	-0.5489	-0.2686
1.0000	2.6000	-0.6807	-0.2628
1.0000	3.1000	-0.8124	-0.2624
1.0000	3.6000	-0.9440	-0.2625
1.0000	4.1000	-1.0755	-0.2628
1.0000	4.6000	-1.2069	-0.2630
31.0000	0.1000	-0.0247	-0.2677
31.0000	0.6000	-0.1561	-40.0377
31.0000	1.1000	-0.1105	-114.3729
31.0000	1.6000	-0.2974	-3.2521
31.0000	2.1000	-0.4587	-0.4454
31.0000	2.6000	-0.6176	-0.2666
31.0000	3.1000	-0.8027	-0.2609
31.0000	3.6000	-0.9440	-0.2627
31.0000	4.1000	-1.0745	-0.2625
31.0000	4.6000	-1.2027	-0.2618
61.0000	0.1000	-0.0196	-0.2726
61.0000	0.6000	-0.1510	-78.5295
61.0000	1.1000	0.0658	-224.8021
61.0000	1.6000	-0.1759	-6.1447
61.0000	2.1000	-0.3740	-0.6227
61.0000	2.6000	-0.6118	-0.2746
61.0000	3.1000	-0.8075	-0.2626
61.0000	3.6000	-0.9369	-0.2621
61.0000	4.1000	-1.0606	-0.2605
61.0000	4.6000	-1.1720	-0.2566
91.0000	0.1000	-0.0112	-0.2775
91.0000	0.6000	-0.1425	-117.0209
91.0000	1.1000	0.2454	-335.2314
91.0000	1.6000	-0.0505	-9.0375
91.0000	2.1000	-0.3044	-0.7920
91.0000	2.6000	-0.6677	-0.2626
91.0000	3.1000	-0.7964	-0.2619
91.0000	3.6000	-0.9218	-0.2606
91.0000	4.1000	-1.0268	-0.2551
91.0000	4.6000	-1.0683	0.3603
121.0000	0.1000	0.0005	-0.2824
121.0000	0.6000	-0.1308	-155.5127
121.0000	1.1000	0.4284	-445.6606
121.0000	1.6000	0.0750	-11.9267
121.0000	2.1000	-0.2594	-0.9307
121.0000	2.6000	-0.6558	-0.2625
121.0000	3.1000	-0.7828	-0.2615
121.0000	3.6000	-0.8826	0.0229
121.0000	4.1000	-0.9047	0.9671
121.0000	4.6000	-0.8196	2.5825
151.0000	0.1000	0.0156	-0.2872
151.0000	0.6000	-0.1157	-194.0044
151.0000	1.1000	0.6147	-556.0898
151.0000	1.6000	0.2010	-14.8088
151.0000	2.1000	-0.2487	-0.9969
151.0000	2.6000	-0.6405	-0.2625
151.0000	3.1000	-0.7252	0.3173
151.0000	3.6000	-0.7774	1.2335
151.0000	4.1000	-0.7276	2.8588
151.0000	4.6000	-0.4552	5.4523
181.0000	0.1000	0.0340	-0.2921
181.0000	0.6000	-0.0973	-232.4925
181.0000	1.1000	0.8043	-666.5191
181.0000	1.6000	0.3266	-17.6779

181.0000	2.1000	-0.2818	-0.9258
181.0000	2.6000	-0.5972	0.0648
181.0000	3.1000	-0.6704	0.8698
181.0000	3.6000	-0.6683	2.3162
181.0000	4.1000	-0.5034	4.7923
181.0000	4.6000	0.0072	8.7059
211.0000	0.1000	0.0558	-0.2970
211.0000	0.6000	-0.0756	-270.9837
211.0000	1.1000	0.9946	-776.9231
211.0000	1.6000	0.4511	-20.5256
211.0000	2.1000	-0.3593	-0.4935
211.0000	2.6000	-0.5511	0.4136
211.0000	3.1000	-0.5882	1.5700
211.0000	3.6000	-0.5281	3.6603
211.0000	4.1000	-0.2083	7.1861
211.0000	4.6000	0.6099	12.6917
241.0000	0.1000	0.0808	-0.3019
241.0000	0.6000	-0.0505	-309.4748
241.0000	1.1000	1.1905	-887.3487
241.0000	1.6000	0.5737	-23.3411
241.0000	2.1000	-0.4242	0.0157
241.0000	2.6000	-0.5013	0.7698
241.0000	3.1000	-0.5151	2.3121
241.0000	3.6000	-0.3692	5.1611
241.0000	4.1000	0.1494	9.9499
241.0000	4.6000	1.3790	17.4817
271.0000	0.1000	0.1092	-0.3068
271.0000	0.6000	-0.0221	-347.9659
271.0000	1.1000	1.3897	-997.7744
271.0000	1.6000	0.6979	-26.0607
271.0000	2.1000	-0.3846	0.1653
271.0000	2.6000	-0.4472	1.1555
271.0000	3.1000	-0.4309	3.1911
271.0000	3.6000	-0.1768	6.9279
271.0000	4.1000	0.5154	13.1728
271.0000	4.6000	2.4332	23.0489
301.0000	0.1000	0.1409	-0.3116
301.0000	0.6000	0.0096	-386.4571
301.0000	1.1000	1.5923	-1108.2001
301.0000	1.6000	0.8192	-28.7170
301.0000	2.1000	-0.3411	0.3229
301.0000	2.6000	-0.3904	1.5726
301.0000	3.1000	-0.3118	4.1805
301.0000	3.6000	0.0427	8.9262
301.0000	4.1000	1.0292	16.8972
301.0000	4.6000	3.3896	29.4260
331.0000	0.1000	0.1759	-0.3165
331.0000	0.6000	0.0446	-424.9482
331.0000	1.1000	1.7981	-1218.6258
331.0000	1.6000	0.9363	-31.2936
331.0000	2.1000	-0.2927	0.4981
331.0000	2.6000	-0.3265	2.0509
331.0000	3.1000	-0.2111	5.2842
331.0000	3.6000	0.2991	11.1982
331.0000	4.1000	1.6341	21.1006
331.0000	4.6000	4.2384	36.6524
361.0000	0.1000	0.2143	-0.3214
361.0000	0.6000	0.0831	-463.4418
361.0000	1.1000	2.0074	-1329.0508
361.0000	1.6000	1.0485	-33.7646
361.0000	2.1000	-0.2416	0.6802
361.0000	2.6000	-0.2377	2.5761
361.0000	3.1000	-0.0595	6.5240
361.0000	3.6000	0.5136	13.7326
361.0000	4.1000	2.2185	25.8127
361.0000	4.6000	5.1433	44.7490
391.0000	0.1000	0.2560	-0.3263
391.0000	0.6000	0.1250	-501.9360
391.0000	1.1000	2.2216	-1439.4669
391.0000	1.6000	1.1550	-36.1009
391.0000	2.1000	-0.1867	0.8791
391.0000	2.6000	-0.1612	3.1580
391.0000	3.1000	0.0628	7.8959
391.0000	3.6000	0.8315	16.5516
391.0000	4.1000	3.0177	31.0409
391.0000	4.6000	6.1071	53.7475

421.0000	0.1000	0.3010	-0.3311
421.0000	0.6000	0.1701	-540.4316
421.0000	1.1000	2.4284	-1549.6475
421.0000	1.6000	1.2550	-38.2699
421.0000	2.1000	-0.1277	1.0959
421.0000	2.6000	-0.0797	3.7966
421.0000	3.1000	0.2511	9.4025
421.0000	3.6000	1.1880	19.6508
421.0000	4.1000	3.9364	36.7932
421.0000	4.6000	7.1308	63.6694
451.0000	0.1000	0.3494	-0.3360
451.0000	0.6000	0.2186	-578.9267
451.0000	1.1000	2.6484	-1660.0504
451.0000	1.6000	1.3477	-40.2349
451.0000	2.1000	-0.0648	1.3316
451.0000	2.6000	0.0068	4.4940
451.0000	3.1000	0.3978	11.0562
451.0000	3.6000	1.5889	23.0395
451.0000	4.1000	4.9848	43.0756
451.0000	4.6000	8.2089	74.5289
481.0000	0.1000	0.4010	-0.3409
481.0000	0.6000	0.2704	-617.4253
481.0000	1.1000	2.8715	-1770.4546
481.0000	1.6000	1.4320	-41.9549
481.0000	2.1000	0.0017	1.5866
481.0000	2.6000	0.0973	5.2514
481.0000	3.1000	0.5509	12.8544
481.0000	3.6000	2.0331	26.7186
481.0000	4.1000	5.9413	49.9073
481.0000	4.6000	9.3421	86.3460
511.0000	0.1000	0.4560	-0.3458
511.0000	0.6000	0.3255	-655.9230
511.0000	1.1000	3.0972	-1880.8593
511.0000	1.6000	1.5066	-43.3833
511.0000	2.1000	0.0882	1.8440
511.0000	2.6000	0.2329	6.0517
511.0000	3.1000	0.7931	14.7822
511.0000	3.6000	2.5235	30.6925
511.0000	4.1000	7.2372	57.2658
511.0000	4.6000	10.5277	99.1374
541.0000	0.1000	0.5143	-0.3507
541.0000	0.6000	0.3839	-694.4220
541.0000	1.1000	3.3264	-1991.2638
541.0000	1.6000	1.5717	-44.4684
541.0000	2.1000	0.1631	2.1379
541.0000	2.6000	0.3367	6.9323
541.0000	3.1000	0.9695	16.8774
541.0000	3.6000	3.0642	34.9640
541.0000	4.1000	8.2590	65.2187
541.0000	4.6000	11.7676	112.9194
571.0000	0.1000	0.5760	-0.3555
571.0000	0.6000	0.4457	-732.9225
571.0000	1.1000	3.5589	-2101.6679
571.0000	1.6000	1.6264	-45.1536
571.0000	2.1000	0.2419	2.4535
571.0000	2.6000	0.4458	7.8778
571.0000	3.1000	1.2577	19.0930
571.0000	3.6000	3.6579	39.5346
571.0000	4.1000	9.1919	73.7667
571.0000	4.6000	13.0609	127.7069

CONTOUR PLOT OF THE SAMPLE PROGRAM OUTPUT

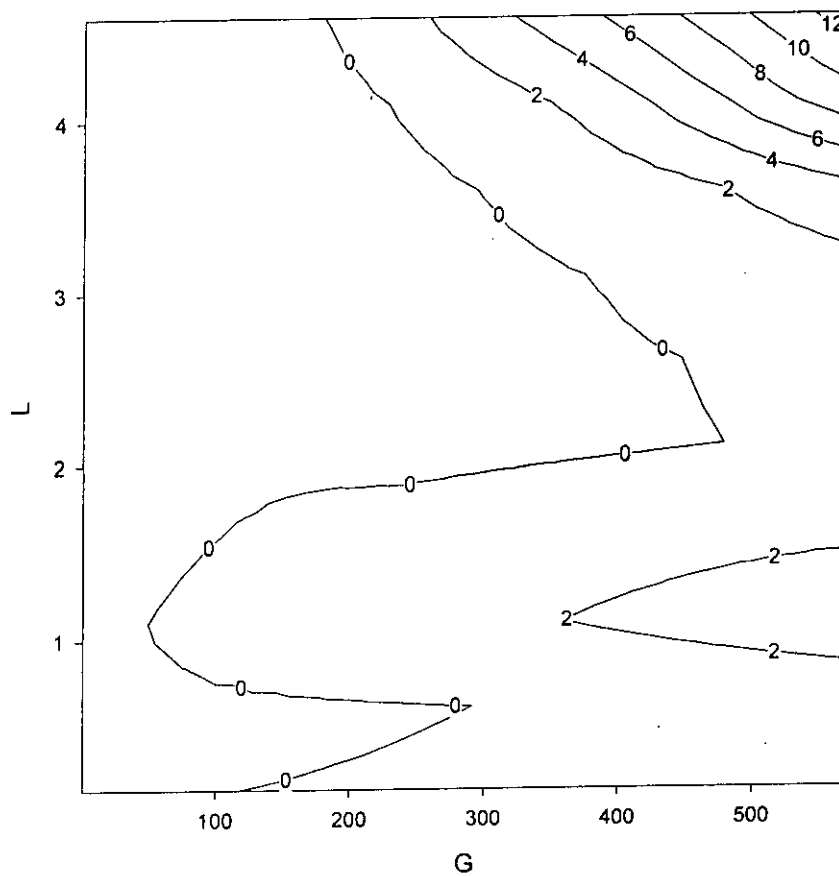
For R113, $L_{he}=840\text{mm}$, $D=7\text{mm}$, $P=0.3\text{MPa}$, $n=2$ 

Fig. C.1 Contour Plot of F1

For R113, $L_{he}=840\text{mm}$, $D=7\text{mm}$, $P=0.3\text{MPa}$, $n=2$

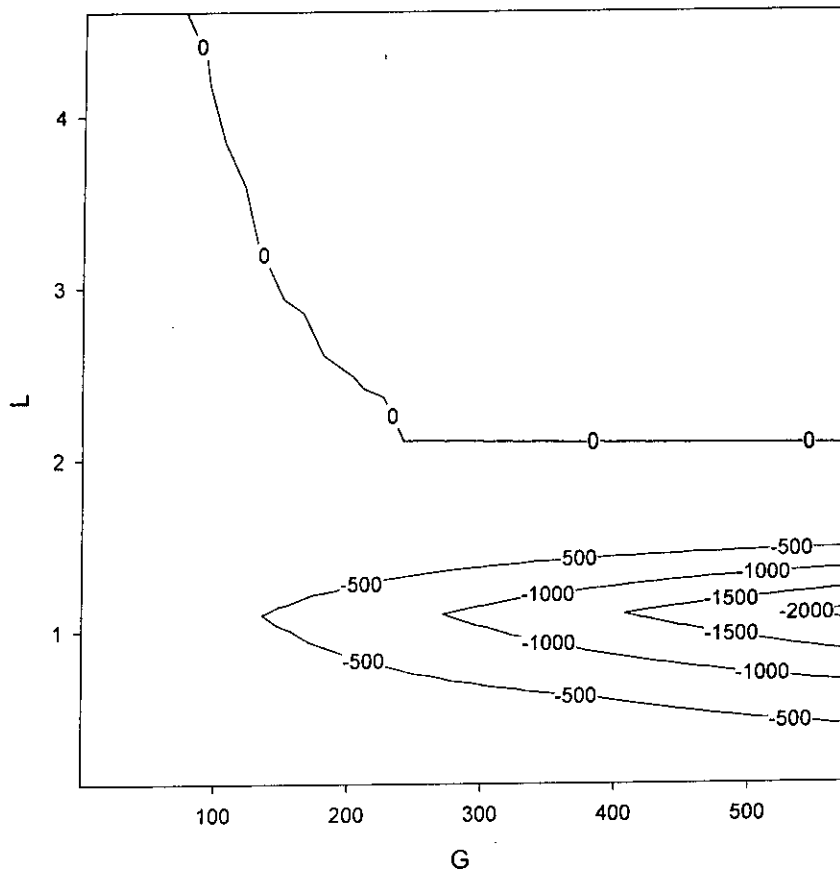


Fig. C2 Contour Plot of F_2

